STRUCTURE AND MECHANICAL PROPERTIES OF DIRECTIONALLY SOLIDIFIED Zn-Al FOUNDRY ALLOYS

Final Report

by

R.W. Smith

Department of Metallurgical Engineering
Queen's University, at Kingston
Ontario, K7L 3N6

Work on this project was conducted under the auspices of the "Physical Metallurgy Research Laboratories, Canada Centre for Mineral and Energy Technology, Energy Mines and Resources, Canada.

DSS File Number: 24SU-23440-3-9008
DSS Contract Number: 24SU-23440-3-9008
CANMET Project: 705402
CANMET Scientific Authority: Dr. M. Sahoo

August 1985

MICROMEDIA

This report should be cited by DSS File No. 24SU-23440-3-9008

Abstract

The solidification behaviour of the new family of Zn-Al alloys (both pure binary and commercial) containing 8, 11 and 27% Al has been examined by the unidirectional solidification technique. The work has been concentrated on understanding the effect of growth direction, growth rate and temperature gradient on the macrosegregation patterns. The mechanical properties of the unidirectionally-grown alloys have been determined and compared with the as-cast values. The effect of some grain refiners, such as Zr, Ti and Ti + B has been evaluated. Finally, the melts of Zn-27% Al alloy have been solidified in an electromagnetic stirrer in order to see the influence of forced-fluid flow on inverted pipe formation. The information generated has been used to develop a generalized description of the freezing of a Zn-Al casting which normally undergoes significant underside shrinkage.

Acknowledgements

This work was performed for the Physical Metallurgy Research Laboratories, CANMET, Energy, Mines and Resources Canada and Supply and Services Canada, contract 24SU-23440-3-9008. The author is indebted to PMRL, CANMET for the preparation of the commercial Zn-Al alloys and for carrying-out the chemical analysis. The various discussion with Dr. M. Sahoo during the course of this work has proved to be invaluable.

All interpretations of data, conditions, etc., are those of the author and his research assistants and do not necessarily reflect the views of CANMET. Crown copyright of this report is reserved.

TABLE OF CONTENTS

	Page
Abstract	i
Acknowledgements	ii
Table of Contents	iii
List of Figures	v
List of Tables	ix
1. Introduction	1
2. Experimental Procedure	4
2.1 Alloy Preparation	4
2.1.1 Directional Solidification	4
2.1.2 Electromagnetic Stirring (EMS)	5
2.1.3 Grain Refinement	5
2.2 Casting Simulation	6
2.3 Mechanical Testing	7
2.4 Apparatus	7
2.4.1 Growth Apparatus	7
2.4.2 Electromagnetic Stirrer	8
3. Results and Discussion	9
3.1 Directional Solidification	9
3.1.1 Microstructures of the Horizontally-Grown Alloys	9
3.1.1.1 Quenched Interfaces	11
3.1.1.2 Decanted Interfaces	13
3.1.2 Microstructures of Vertically-Grown Alloys	14
3.1.2.1 Solid-down Growth	15
3.1.2.2 Solid-up Growth	17

3.1.2.3 Quenched Interfaces 18

3.2 Casting Simulation 21

3.3 Mechanical Properties of Directionally-Solidified Alloys ... 22

3.4 Additions of Grain Refiners 23

3.4.1 The Effect of Ti 23

3.4.2 The Effect of Zr 24

3.4.3 The Effect of Ti + B 25

3.4.4 Directionally-Solidified Alloys with the Additions of Ti and Zr 26

3.5 Electromagnetic Stirring 26

3.5.1 Small-size Ingots (3 lb) in Sand Molds 27

3.5.2 Small-size Ingots (3 lb) in Heated Ceramic Molds 28

3.5.3 Large Ingots (8 1/2 lbs) in Shell Molds 28

3.5.4 Chemical Analyses and Metallographic Studies on the Unstirred and Stirred Ingots 30

3.6 Development of Underside Shrinkage in Sand Castings 31

4. Conclusions 34

References 36

Appendix 38

LIST OF FIGURES

Fig. 1. The binary Zn-Al equilibrium diagram. The first solid to form in the Zn-27%Al alloy is 60%Al

Fig. 2. Schematic cross-section Al representation of the casting (i.e. solid-down case) with thermocouple positions

Fig. 3. Crystal growers (a) vertical; (b) horizontal

Fig. 4. (a) Schematic drawing of the mechanical cross-section of the stirrer and field strengths in milli-teslas
(b) Force distribution (end view)
(c) Idealized fluid flow pattern

Fig. 5. Longitudinal sections (5mm dia.) of horizontally-grown Zn-11%Al alloy, R(growth rate) = 5×10^{-3} cm/sec, G(temperature gradient) = 10°C/cm.

(a) start-end, (b) central section, (c) finish-end (x16)

Fig. 6. Longitudinal sections (5mm dia.) of horizontally-grown alloys (central sections), R = 5×10^{-3} cm/sec, and G = 10°C/cm.

(a) Zn-8%Al, (b) Zn-27%Al (x16)

Fig. 7. Central longitudinal sections of the alloys grown horizontally (10mm dia.), R = 5×10^{-3} cm/sec, and G = 10°C/cm.

(a) Zn-8%Al, (b) Zn-11%Al, (c) Zn-27%Al (x6)

Fig. 8. Longitudinal section of the quenched interface of the Zn-27%Al alloy grown horizontally (5mm dia.), R = 5×10^{-3} cm/sec, G = 10°C/cm. (x10).

Fig. 9. Bottom surfaces of the decanted alloys grown horizontally R = 5×10^{-3} cm/sec. (x2).

Fig. 10. Microstructures of the Zn-8%Al alloy grown vertically upwards. 5mm dia. (left), 10mm dia. (right), R = 5×10^{-3} cm/sec, G = 44°C/cm. (x100).

Fig. 11. Microstructures of the Zn-8%Al alloys grown vertically upwards (5mm i.d.),

R = 10^{-2}cm/sec, G = 62°C/cm (left)

$R_2 = 10^{-1}$cm/sec, G_2 = 20°C/cm (right). (x100).

Fig. 12. Microstructures of the Zn-11%Al alloys grown vertically upwards (5mm i.d.).
(a) R = 10^{-3}cm/sec, G = 44°C/cm, (b) R = 10^{-2}cm/sec, G = 62°C/cm,

(c) R = 10^{-1}cm/sec, G = 20°C/cm. (x100).

Fig. 13. Microstructures of the Zn-27%Al alloy grown vertically upwards (5mm i.d.).

(a) $R = 10^{-3}$cm/sec, $G = 44°C/cm$, (b) $R = 10^{-2}$cm/sec, $G = 62°C/cm$,

(c) $R = 10^{-1}$cm/sec, $G = 20°C/cm$. (x100).

Fig. 14. Microstructures of the ZA-8 (commercial) alloy, $R = 5 \times 10^{-3}$ cm/sec.

(a) Solid-down, $G = 44°C$. (b) Solid-down, $G = 56°C$. (x100).

Fig. 15. Microstructures of the Zn-8%Al alloy grown vertically downwards. 5mm i.d. (left), 10mm i.d. (right). $R = 5 \times 10^{-3}$ cm/sec, $G = 56°C/cm$. (x100).

Fig. 16. Microstructures of the Zn-8%Al alloy grown vertically downards (5mm i.d.) left ($R = 10^{-2}$cm/sec, $G = 62°C$), right ($R = 10^{-1}$cm/sec, $G = 20°C/cm$. (x100).

Fig. 17. Microstructres of the Zn-11%Al alloy grown vertically downwards (5mm dia.)
(a) $R = 5 \times 10^{-3}$cm/sec, $G = 56°C/cm$ (b) $R = 10^{-2}$cm/sec, $G = 62°C/cm$ (c) $R = 10^{-1}$cm/sec, $G = 20°C/cm$. (x100).

Fig. 18. Microstructres of the Zn-27%Al alloy grown vertically downwards (5mm dia.)
(a) $R = 5 \times 10^{-3}$cm/sec, $G = 56°C/cm$ (b) $R = 10^{-2}$cm/sec, $G = 62°C/cm$ (c) $R = 10^{-1}$cm/sec, $G = 20°C/cm$. (x100).

Fig. 19. Microstructres of the alloys grown vertically downwards (5mm dia).

$R = 5 \times 10^{-1}$cm/sec, $G = 250°C/cm$ (a) Zn-8%Al, (b) Zn-11%Al, (c) Zn-27%Al. (x100).

Fig. 20. Longitudinal sections of quenched interfaces of the Zn-8%Al alloys (5mm dia.)
$R = 5 \times 10^{-3}$cm/sec. (a) solid-down, $G = 44°C/cm$ (x14)
(b) solid-up, $G = 56°C$ (x14).

Fig. 21. Longitudinal sections of quenched interfaces of the Zn-11%Al alloys (5mm dia.)
$R = 5 \times 10^{-3}$cm/sec. (a) solid-down, $G = 44°C/cm$
(b) solid-up, $G = 56°C$ (x13).

Fig. 22. Longitudinal sections of quenched eutectic interfaces (5mm dia.), $R = 5 \times 10^{-3}$ cm/sec. (a) Zn-8%Al, solid-up, $G = 56°C/cm$. (x400).
(b) ZA-8, solid up, $G = 120°C/cm$ (x400).

Fig. 23. Longitudinal sections of the quenched interface of the Zn-27%Al alloy. $R = 5 \times 10^{-3}$ cm/sec, (a) solid-down, $G = 44°C/cm$ (x13)
(b) solid-up, $G = 56°C/cm$ (x13), (c) solid-up, $G = 120°C/cm$.

Fig. 24. Longitudinal sections of the quenched interfaces of the commercial alloys grown vertically upwards. $R = 5 \times 10^{-3}$ m/sec, G = 44°C/cm (x12) (a) ZA-8, (b) ZA-11, (c) ZA-27.

Fig. 25. Schematic drawings of the different casting configurations (ZA-27 alloy) with Al-concentration at various points.
(a) solid-down (b) solid-up (c) horizontal

Fig. 26. Cooling curves (a) without chill (b) with chill.

Fig. 27. SEM Micrograph of the fracture surface of the Zn-11%Al alloy.

Fig. 28. Microstructures of the ZA-12 (commercial) alloy
(a) Sand-cast (x100), (b) Chill-cast (x100),
(c) SEM (Sand-cast), (d) SEM (Chill-cast).

Fig. 29. Microstructures of the ZA-12 + 0.05% Ti alloy
(a) Sand-cast (x100), (b) Chill-cast (x100),
(c) SEM (Sand-cast), (d) SEM (Chill-cast).

Fig. 30. Microstructures of the ZA-27 (commercial) alloy
(a) Sand-cast (x100), (b) Chill-cast (x100),
(c) SEM (Sand-cast), (d) SEM (Chill-cast).

Fig. 31. Microstructures of the ZA-27 + 0.05% Ti alloy
(a) Sand-cast (x100), (b) Chill-cast (x100),
(c) SEM (Sand-cast), (d) SEM (Chill-cast).

Fig. 32. Nucleating particle (Al_5Ti_2Zn) at the center of the primary Al-rich dendrite.
(a) low magnification
(b) high magnification.

Fig. 33. Microstructures of the ZA-12 + 0.05% Zr alloy
(a) Sand-cast (x100), (b) Chill-cast (x100),
(c) SEM (Sand-cast), (d) SEM (Chill-cast).

Fig. 34. Microstructures of the ZA-27 + 0.05% Zr alloy
(a) Sand-cast (x100), (b) Chill-cast (x100),
(c) SEM (Sand-cast), (d) SEM (Chill-cast).

Fig. 35. Microstructures of the ZA-12 + 0.065% Ti + 0.013% B alloy
(a) Sand-cast (x100), (b) Chill-cast (x100),
(c) SEM (Sand-cast), (d) SEM (Chill-cast).

Fig. 36. Microstructures of the ZA-27 + 0.065% Ti + 0.013% B alloy
(a) Sand-cast (x100), (b) Chill-cast (x100),
(c) SEM (Sand-cast), (d) SEM (Chill-cast).

Fig. 37. Green sand mold: 1- Non-stirred 2- Stirred immediately after pouring.

Fig. 38. Ceramic mold (heatd up to 600°C)
A non-stirred B stirred with the magnetic force downward
C stirred with the magnetic force upward

Fig. 39. Large size ingots: a - Longitudinal section b - Side view.

Fig. 40. Longitudinal section of ingots of the Zn-27%Al showing the locations of samples taken by drilling for chemical analyses
(a) unstirred ingot (A1) (b) stirred ingot (Q4).

Fig. 41. Micrographs from the various positions in the unstirred ingot (see Fig. 33A)
(a) The spot number 7 (i.e. the top of the ingot)
(b) The spot number 1 (i.e. the bottom of the ingot). (x100).

Fig. 42. Micrographs from the various positons in the unstirred ingot (see Fig. 33B).
(a) The spot number 8 (i.e. the top of the ingot)
(b) The spot number 1 (i.e. the bottom of the ingot). (x100).

Fig. 43. Schematic illustration of the solid liquid interface in a casting.

LIST OF TABLES

Table 1: Comparative properties of foundry alloys

Table 2: Composition of the commercial alloys (wt %)

Table 3: Composition (wt %) of the sand-cast test bars in the commercial alloys

Table 4: Composition in various positions of the unidirectionally-solidified rod. (Zn-27%Al alloy)

Table 5: Mechanical properties of the directionally-grown binary alloys

Table 6: Mechanical properties of the directionally-grown commercial alloys

Table 7: Mechanical properties of the commercial alloys (sand-cast Dow test bars)

Table 8: Composition in various positions of the stirred and un-stirred ingots (Zn-27% Al alloy)

1. Introduction

Traditionally, zinc has been used primarily as a coating to protect steel against corrosion; however, die casting applications represent the second major use. With respect to the latter, zinc alloys were developed and used in Germany during World War II as bearing materials, being substituted for bronze because of copper scarcity. Extensive foundry applications of the zinc alloys only started relatively recently [1-2]. High impurity contents (i.e. Pb, Sn, Cd, Bi, Hg, In, Ag, Sb, and Tl) made the early zinc alloys susceptible to intergrannular corrosion [3-5]; this initial set-back has affected the more general usage of Zn-Al alloys.

Starting from the early 1960's, ZA-12, ZA-27 and ZA-8* alloys were developed progressively for sound castings and general foundry use in the United States and Canada. These alloys, with excellent foundry and mechanical characteristics, have reduced the cost of subsequent finishing operations and have achieved considerable success in the non-ferrous foundry technology. The mechanical properties of the alloys are comparable with more traditional alloys both ferrous and non-ferrous (See Table 1), often with substantial weight savings.

However, the most promising alloy, ZA-27, has a very long freezing range (112°C) [6-7] and therefore it is difficult to produce sound castings with this alloy. Unlike the other alloys, a casting of this alloy tends to

---

*The digits reflect the approximate aluminum content of the alloy, given in wt%. Throughout the text, designations starting with ZA refer to commercial Zn-Al alloys which also contain Mg and Cu.

shrink from the bottom to the top during freezing. It has been thought that the considerable density difference between the Al-rich primary phase and the Zn-rich liquid phase is responsible for the inverted pipe formation (see fig. 1). The size of such a defect in ZA-12 and ZA-8 alloys is found to be less than in the ZA-27 alloy, but is strongly dependent upon pouring temperature, thermal gradients and cooling rates, and the feeding of the casting [6-8].

Recently, videotape observations of the solidification in the ZA-27 alloy showed that the shrinkage occurs while the alloy is 75% to 90% solid [9]. Habiby and McNallan also suggested that the problem may be controlled by changing the macrosegregation patterns in the casting through the use of chills and risers [9].

In the early 1960's, several researchers studied the effects of small additions of Ni, Ti, Mn, Zr, Be and Li on the structure and mechanical properties of zinc-aluminum binary alloys [10] and Zamak series alloys [11-12]. During the last decade, Pollard, et al [13-14] showed that additions of not less than 0.04 wt% of Ti to Zn-Al alloys containing 7 to 24 % Al is sufficient for complete grain-refinement of the primary Al-rich phase. Sahoo, et al [7] indicated that a gating ratio of 1:5:3 and a Ti content of 0.05 to 0.1% appears to maximize the improvement in casting quality although some underside shrinkage was still present. They also concluded that addition of Ti does not improve the elongation of all three alloys and, in some cases, the UTS and YS seemed to be adversely affected. A more detailed work [15] dealt with the effect of grain-refining additions (B, Ti, Zr, La, Ce, and B + Ti) on the microstructures and mechanical properties of the Zn-Al alloys. It was found that substantial increases in

ductility were achieved by the additions of (B + Ti), La or Ce. (B+Ti) also improved the tensile strength and ductility level of ZA alloys substantially while maintaining the other properties of the alloys practically unchanged [15]. It was also observed that Zr refined the microstructures, but did not effect the mechanical properties.

The latest attempt to control the underside shrinkage in these alloys by the addition of trace elements (i.e. group 1A and IIA elements) has been made by Sahoo et al [16]. In this it was found that Be, Ca, Sr, Ba, Li, K, Cs and Na helped to eliminate underside shrinkage in 25 mm thick plate castings, although the precise manner in which this was achieved was not clear.

The aim of the present work is first to develop a better understanding of the solidification behaviour of the Zn-Al alloys and, perhaps, to use this understanding to solve the underside shrinkage problem. The solidification behaviour of these alloys has been examined by the unidirectional solidification technique (both vertical and horizontal). Hence, this work has concentrated on understanding the effects of growth rate, growth type and temperature gradient on the macrosegregation patterns. Whilst particular attention has been directed towards the pure binary alloys (Zn-8%Al, Zn-11%Al, and Zn-27% Al), some experiments have also been carried out with the commercial alloys (ZA-8, ZA-12, and ZA-27). An attempt has been made to determine the mechanical properties of the unidirectionally grown alloys, as well. The effects of some grain-refiner used in the past, such as Zr, Ti, and (Ti+B) have been evaluated.

Finally, melts of Zn-27% Al alloy were solidified in an electromagnetic stirrer under various conditions in order to see the influence of the forced-fluid flow on inverted pipe formation.

2. Experimental Procedure

2.1 Alloy Preparation

2.1.1 Directional Solidification

Materials:

For pure binary alloys, the materials used were 99.99% Zn, and 99.99+ % Al. Alloys were also prepared to commercial specifications at CANMET Laboratories in Ottawa (See Table 2).

Melting Practice and Casting:

The melting of the alloys was performed in a resistance-heated furnace using clay graphite crucibles coated with alumina. Since Al does not dissolve very easily in molten Zn, first Al was melted and then Zn was added to the molten Al.

The liquid metal temperature was always kept below 700°C in order to reduce possible Zn fuming. Prior to casting, the liquid alloys were stirred with an alumina coated graphite rod and poured into the brass and cast iron chill molds at 600°C.

The commercial alloys (ZA-8, ZA-12, and ZA-27), supplied by CANMET, were remelted and cast into the brass and cast iron chill molds under one atmosphere of argon in a BALZERS vacuum induction unit in order to prevent oxidation and composition shift.

Specimen Tube Filling:

Since the liquidus temperatures of the alloys are in the softening

range of Pyrex glass, it is necessary to carry-out the experiment in Vycor glass tubing. In practice after being sealed at one end, the inner surface of tubes was coated with (spray-)graphite.

All the alloys were chill cast in a rod shape and were swaged to a diameter slightly less than the inner diameter of the growth tube, then placed in a coated Vycor tube. Following this, the tube was roughly evacuated and flushed with argon several times, to be sealed under a partial pressure of argon to reduce zinc evaporation.

2.1.2 Electromagnetic Stirring (EMS)

The materials used were 99.99% Zn, and 99.8% Al. Melting was done in an induction furnace employing clay graphite crucibles. The same melting procedure was followed as mentioned in the previous section. Three different types of molds were utilized: green sand, ceramic, and resin-shell molds.

The green sand molds were prepared in synthetic silica sand (AFS fineness 60-70) with 4% bentonite, 4% moisture in a non-magnetic stainless steel container. The shell molds were also prepared in the same container from resin-setting washed silica sand (baked at 200°C for an hour). The ceramic molds were produced by an investment moldings technique, and then placed into the same stainless steel container. For each case, the pouring temperature was 600°C, and the ceramic molds were heated up to 600°C before casting.

2.1.3 Grain Refinement

Commercial alloys supplied by CANMET were utilized. Ti, Zr and

(Ti+B) were added as commercial Al-6.2% Ti, Al-5.4%Zr, and Al-5%Ti-1%B master alloys in amounts ranging from 0.02 to 0.065 wt%. Melting was carried out in a resistance heating furnace using the clay-graphite crucibles. The melt was kept at 650°C for an hour in order to ensure the complete dissolution of the master alloys, and then poured into green sand and brass chill molds at 600°C after stirring vigorously. Later some of the chill bars were also grown unidirectionally in Vycor tubes following swaging.

2.2 Casting Simulation

Unidirectional solidification was intended to simulate the freezing of small-size castings. Three casting configurations (solid-up, solid-down and melt horizontal) were used: each in two conditions, namely, "with chill" and "without chill". The ZA-27 (commercial) alloy was used in these experiments.

The melts were cast into sand molds. Riser sleeves were used to form the casting cavity in order to achieve directional heat removal. A cast iron chill was placed at one end of the casting cavity so that solidification started from that end and progressed towards the other end. The weight of the chill was approximately equal to five times that of the casting. In the "without chill" mold, the chill block was replaced by sand (see fig. 2).

Some thermal analyses were also performed in the solid-down case "with" and "without" a chill. In order to determine the temperature gradient created in the liquid, a number of thermocouples were located

along the vertical axis of the molds at distances of 30 mm, 60 mm, and 90 mm from the mold base (see fig. 2 for the positions of the thermocouples).

2.3 Mechanical Testing

Tensile specimens were machined from both the unidirectionally-grown and chill cast binary alloys. Following a number of premature failures during tensile testing, prior to machining the tensile specimens the crystal rods were examined for internal porosity and flaws by X-radiography. A number of rods were found to contain defects and thus were re-grown. Because of this, considerably more time had to be expended than initially anticipated to prepare satisfactory samples. Therefore, only a small number of successful tests have been performed.

Compression samples were machined from the unidirectionally-grown pure binary and commercial alloys. Some compression tests were also done on the sand-cast alloys which were supplied by CANMET Laboratories (see table 3). All the tests were carried-out on an 'INSTRON' testing machine. The values given are the average of three test results unless it is indicated otherwise.

2.4 Apparatus

2.4.1 Growth Apparatus

In principle, the crystal grower was of the Bridgman-type with a resistance heating furnace (fig. 3a). The vertical grower was capable of growth rates between 10^{-6} and 10^{-1} cm/sec for growth directions both vertically upwards and downwards. To monitor the temperature gradient, three different quench-baths were attached to the unit: i.e. air, water,

and a tightly fitting watercooled copper cylinder. This gave respectively, small, medium and large temperature gradient quench baths. The quenched interfaces were produced by either pulling the growth tube rapidly further into the quench-bath or dropping the growth tube into a water container in order to delineate the S/L interface morphology, while the run was in progress.

The horizontal grower was essentially the same as the vertical one (fig. 3b). The only difference was that the components were placed on a horizontal frame which was inclined 5° to the horizontal in order to keep the liquid in full contact with the solid. In this case, the growth tube was held stationary while the furnace moved. The quenched interfaces were obtained by moving the furnace rapidly away then pouring cold water on the growth tube. The decanted interfaces were produced in a graphite boat within a silica tube. The unit was sealed with flanges at the two ends which allowed the graphite boat to turn freely inside the silica tube. When the sample was grown to a predetermined length under an argon atmosphere, the boat was tilted 180° by turning the flange in order to permit the remaining liquid to fall away from the solid.

2.4.2. Electromagnetic Stirrer

The electromagnetic stirrer employed in this project was a linear induction pump. This is essentially a tubular linear induction motor (TLIM). It contained three cylindrical copper coils potted in epoxy. These coils were connected to each other in such a way that the resultant magnetomotive force (MMF) became longitudinal and its magnitude (intensity)

decreased towards the centre of the bore. This created a continuous movement within the e melt. The MMF experienced by the sample was a function of time and position inside the stirrer. This created a continuous movement within the melt. Fig. 4 shows the mechanical cross section of the stirrer, and the idealized fluid flow patterns produced (see Appendix I for more detailed information).

3. Results and Discussion

This part of the report is divided into three main sections. Section 3.1 discusses the effects of different growth types on the microstructure, segregation patterns and mechanical properties. Section 3.4 deals with the structural modification through impurity additions. Finally, Section 3.5 relates to the effects of the forced fluid flow on the inverted pipe formation.

3.1 Directional Solidification

3.1.1 Microstructres of the Horizontally Grown Alloys

In order to have a better understanding of the possible gravity segregation occurring in the Zn-Al alloys, the pure binary (Zn-8% Al, Zn-11% Al, Zn-27% Al) alloys were frozen horizontally in 5 and 10 mm i.d. Vycor tubes at a growth rate of 5×10^{-3} cm/sec with a temperature gradient in the liquid of 10°C/cm.

The longitudinal sections of the as-frozen alloys are shown in figs. 5-7. Three sections are given for the Zn-11%Al grown in a 5 mm i.d. tube, namely, start-end, central-position, and the finish-end (see fig. 5).

Solidification started with the nucleation of many cells, which was followed by rapid freezing at the beginning. After a certain amount of growth had taken place, directional heat removal in the solid became possible and marked directionality in the primary dendrites arose (see fig. 5a).

It was observed that the primary (Al-rich) dendrites tended to be inclined, to the horizonal axis, i.e., they seemed to grow upwards away from the S/L interface. The reason for this is not clear, but the buoyancy force on the low density primaries would promote such bending. At the very beginning of solidification, the forward growth of the primaries may predominate and the evolution of the latent heat may prompt non-uniform radial growth, therefore, the main stem stays thinner where it is attached to the general interface. This would make the buoyancy forces more effective, causing dendrite inclination. However, it could be compounded with the tendency of dendrites to grow into the fluid flow [17]. The macroscopic shape of a S/L interface governs the orientation of solidification forms (such as dendrites), since "stable growth" occurs normal to the freezing front and parallel to the temperature gradient. On the contrary, the non-radial columnar growth occurs in an ingot when convective flow sweeps past the S/L interface. By suppressing fluid motion, the interface can be made vertical and the columnar grains grow radially [18]. The reason of this growth direction alteration is not altogether clear, but Chalmers has suggested that heat flow, not solute flow may control the morphologies [17].

It was also observed that the proportion of the Zn-rich liquid (i.e. for the Zn-8% Al and Zn-11% Al alloys it is the eutectic) on the lower side of the specimen increased progressively along the specimen towards the

"finish-end". This became a dendrite-free band on the bottom surface of the specimen in Zn-8% Al and Zn-11% Al alloys (see fig. 5-7). Indeed, macrosegretation (i.e. non-uniform dopant or solute distribution which depends on the scale of the sample) generaly occurs when an impure metal or alloy is solidified unidirectionally from a melt of an initial uniform concentration. The solute partition depends upon the transport conditons in the melt, and may cause different instantaneous concentration profiles in front of the interface as well as different segregation patterns in the solidified crystal. Because of this, the finished-end of the samples contained more Zn-rich liquid eutectic.

Convective processes in melts can produce a wide variety of spatial and temporal variations in transport rate which can yield undesirable macrosegregation and microsegregation patterns in the growing crystal. The solute distribution in crystals depends to a large extent on convective processes existing in the liquid phase. Convective flows are both natural (density-gradient driven), and forced (artificial due to (say) EMS). These flows provide very important sources of enhancing mass transfer in solution growth systems. They are useful in so far as they promote stirring. In general, thermal convection has been shown to exist always as a steady circulation in any liquid where the temperature gradient is not aligned in the direction of gravity.

3.1.1.1 Quenched Interfaces

Since the microstructures gave clear evidence of macro-segregation, the alloys (in 5mm i.d. tubes) were quenched (as described in section 2.2.1) during growth in order to delineate the topography of the S/L interface.

For all the alloys, the interface had an interesting feature. The presence of convection in the liquid had a vital effect on the development of the microstructure. Besides causing variations in the diffusion boundary layer, macrosegregation patterns, and growth fluctuations (banding), it also influences the S/L interface morphology (making it non-planar, fig. 8). Since the colder bulk liquid is stable at the bottom side of the container during horizontal growth. This causes the interface to be convex in the growth direction.

It should be noted that it was dished in an opposite fashion as compared with the more common dishing effect observed during horizontal growth. This could be attributed to the segregation pattern occurring during growth. The Zn-rich denser liquid, having a lower freezing temperature, stayed as liquid to a certain distance behind the dendritic front; this distance was determined by the temperature gradient present in the melt (Fig. 8). In the Zn-8% Al and Zn-11% Al alloys, that point corresponded to the eutectic temperature, so that during quenching the bulk liquid solidified and revealed the eutectic interface in the dendritic network. In this aspect, there was no significant difference between the quenched interfaces of these two alloys, except in the distance the dendritic tips extended beyond the eutectic front. These distances were respectively 4.5 and 7.0 mm. As expected, this distance was more than 20 mm in the Zn-27 %Al alloy owing to extremely mushy solidification. The S/L interface of this alloy dished into the frozen alloy without showing any sharp boundary between the solid and liquid (Fig. 9). It was not possible to see the eutectic interface in the tight dendritic network. These values make sense if the solidification ranges of the alloys are considered. Thus

the mushy zone lengths of the alloys under the given growth conditions corresponded to freezing ranges of 29°, 55° and 112° for the Zn-8Al, Zn-11Al and Zn-27Al alloy, respectively.

3.1.1.2 Decanted Interfaces

The segregation patterns occurring in the Zn-Al alloys were described in the previous sections. The possible mechanisms which control the segregation patterns were also suggested on the basis of metallographic studies. Nevertheless, the information deduced from the longitudinal and transverse sections of the grown and quenched samples was limited to the two dimensional micrographs. It was thought that a three dimensional view of the S/L interface would be captured by producing a decanted interface.

The decanted interfaces were obtained by a method which was described in a detailed manner in section 2.2.1. Fig. 9 indicates the bottom surfaces of the decanted alloys grown horizontally. Upon inverting the specimens during growth to allow the melt to separate from the S/L interface, some of the interdendritic liquid also drained through the dendritic mesh. The remaining liquid solidified in the mushy zone, revealing a sharp transition from the fully solid to the earlier mushy condition because of the lack of feeding to compensate the solidification shrinkage. This was most pronounced for the Zn-8% Al alloy since it contained more eutectic liquid than the other alloys. Besides that, the dendritic network was not as tight as the networks in the other alloys. This allowed the interdendritic liquid to drain easily during decanting.

In the Zn-11% Al and Zn-27% Al alloys, as the freezing range and the mushy zone length increases, the dendritic network gets "tighter".

Therefore, it becomes more difficult for the liquid to drain through the dendrite mesh. Because of this, the areas closer to the dendritic front sank more, exposing the primary dendrites aligned in the growth direction. The rest of the liquid flowed backwards to equalize the solidification shrinkage. As a consequence of this, the sharp transition from the fully solid to the mushy zone was less clearly seen. In the Zn-11% Al alloy the transition was seen, but not as clearly as in the Zn-8% Al alloy (Fig. 9).

3.1.2 Microstructures of Vertically-Grown Alloys

The convective processes existing in liquid alloys are often responsible for the undesirable macrosegregation patterns and deleterious properties of castings. However, these processes may be useful as long as they promote stirring [19]. They can be controlled or eliminated in various ways. As mentioned in earlier sections, convective flows can be both natural and forced. It was also mentioned that thermal (natural) convection would exist as a steady circulation in any liquid where the temperature gradient was not aligned in the direction of gravity (horizontal growth). In the case of vertically-upwards growth, the temperature gradient is parallel to the gravitational field. So is the fluid density gradient. Under these circumstances a motionless solution formally satisfies the fluid flow equations. However, if there is a horizontal density gradient then convective flow may result. By contrast, during vertically downwards growth, there will be vigorous thermosolutal convection in the melt of the Zn-Al alloys (i.e. caused by simultaneous temperature and concentration gradients). This section will discuss the effects on macrosegregation of these two growth types with different

temperature gradients and growth rates.

3.1.2.1 Solid-Down Growth

The pure binary alloys were grown vertically upwards in 5 and 10 mm i.d. Vycor tubes at growth rates of 10^{-1}, 10^{-2} and 5×10^{-3} cm/sec with various temperature gradients (between 20 to 250°C/cm). The temperature gradient was maintained by using both air- and water-quench baths. In some cases the alloys were grown in 17 mm i.d. Vycor tubes to see the effect of the container size on the segregation pattern.

Again, the microstructures showed in an obvious segregation pattern for each alloy (see figs. 10-13). The lower section of the specimen contained more Zn-rich liquid (i.e. the eutectic mixture in the Zn-8% Al, and Zn-11% Al alloys) than the top section. The presence of the coarser primary dendrites in the top portion of the sample was another noticeable feature of the microstructures.

These two features can easily be explained by considering the characteristics of this growth type. Presumably, during growth, the bulk liquid stayed relatively quiescent, since Zn would be the rejected element and so make the solute boundary layer ahead of the interface denser as long as there was no horizontal gradient due to the container size. However, any aluminum dendrite detachment would promote some stirring. As mentioned in the previous section, convective processes could enhance macrosegregation in the crystal. In this case, they were eliminated or at least reduced by placing the S/L interface in a horizontal plane and the hot liquid over the solid. However, two important mechanisms may come into the play in the Zn-Al alloys. The first one is the floating off of any of

the primary Al-rich dendrites which may become detached from the interface. This mechanism can be very effective in quiescent melts [20]. During solidification, the hotter liquid flows into the mushy zone to compensate for the solidification shrinkage. This may cause instabilities and the remelting of the small dendrite stems so that bits of dendrites become detached from the interface (i.e. they are lighter than the surrounding liquid in this case) and so may float towards the top of the melt as a result of the buoyancy forces present. During this process, either they may remelt which increases the local Al-concentration or they may survive and coarsen (figs. 10-13).

The second mechanism is the interdendritic fluid flow taking place in the mushy zone. It is believed that the interdendritic fluid flow is the predominant factor in producing microsegregation in cast alloys [21]. In the Zn-Al alloys, the denser and colder liquid ahead of the interface flows through the interdendritic channels and settles down at the bottom portion of the sample (figs. 10-12).

As expected, the combination of high growth rate and temperature gradient refined the microstructure, therefore the dendritic channels became narrow and the resistance to the interdendritic flow increased. As might be expected, this lead to a relatively reduced segregation throughout the specimen. (figs. 11, 12b and c, 13).

The commercial alloys indicated the same feature as the pure binary alloys as far as the microstructures were concerned (see fig. 14). The only difference was the fineness of the microstructures in the commercial alloys. In these alloys, the microstructures became finer, probably due to the presence of impurities. The impurities (i.e. alloying additions such as Cu, Mg) might promote constitutional undercooling, causing the finer

structure scale.

It was observed that the specimen tube size did not have any significant effect on either the segregation pattern or the microstructure (see fig. 10). However, at very small growth rates and temperature gradients, an internal pore developed throughout the entire sample of the Zn-27%Al alloy grown in a 17mm i.d. tube. This was presumably due to feeding difficulties.

3.1.2.2 Solid-Up Growth

The alloys were grown vertically downwards (i.e. liquid below solid) at growth rates of 10^{-1}, 10^{-2} and 5×10^{-3} cm/sec. To monitor the temperature gradient during growth, both air and tight-fitting quench baths were employed.

Only slight differences in microstructures were observed (See Figs. 15-18), namely, a gradual change in primary dendrite proportions from top to bottom.

Generally speaking, the convection existing in the melt is believed to be the cause of microsegregation. In some cases, vigorous convection may help to homogenize the melt composition. When growth is vertically downward, it is expected that the hotter and lighter liquid is always below the colder and denser liquid. This will cause vigorous thermal convection. Probably, it evens-up the liquid composition all the time and the microstructure ends up with a more uniform chemical composition (See Table 4).

Another factor, dendrite detachment and floating in the quiescent bulk liquid pool, which may be very pronounced in upward growth, cannot be

possible in downward growth since the solid is always over the liquid. If dendrites detach they can only be swept into the melt by the convection currents. This will also help to homogenize the melt (See Table 4).

The combination of large growth rate and temperature gradient refined the microstructure, thus macrosegregation seemed to be much reduced especially with the use of a more tightly fitting quench bath and a growth rate of 10^{-1} cm/sec (see fig. 19). In this case, tertiary arms completely disappeared and even secondary arms did so in some regions. However, the aligned-composite growth at off-entectic composition, first demonstrated demonstrated by Mollard and Flemings [22], did not occur.

As in the solid-down growth, the solid-up growth macrosegregation seemed to be independent of tube diameter for those diameters studied, i.e. 5 and 10 mm. However, the microstructural scale became coarser (fig. 15).

As noted earlier, the principal feature of the vertically-grown commercial alloys was a structural refinement.

3.1.2.3 Quenched Interfaces

In order to delineate the topography of the S/L interface, samples of both the pure binary and commercial alloys were quenched in 5 mm i.d. tubes during growth.

In the previous sections, the segregation patterns developed in the specimens during solid-up and solid-down growth cases were discussed. In general, solid-up growth yielded more uniform microstructures as far as the volume fraction of the primary dendrites was concerned. The results of the quenched-interface experiments will now be discussed.

Solid-Down Specimens

At the first glance, the common feature of the S/L interfaces was the nonplanar dendritic front (see figs. 20-23). In the Zn-8% Al, and Zn-11% Al alloys, the dendritic front was well-defined, but did not proceed in a planar fashion during solidification. Besides that, having off-eutectic compositions, the Zn-8% Al and Zn-11% Al alloys indicated the eutectic front behind the dendrite tips. The morphology of the eutectic interface was essentially cellular (fig. 22). In the Zn-27% Al alloy, no clear indication of the S/L interface was obtained (see fig. 23). The Zn-rich liquid flowed down and stayed between the primary dendrites. Although the quenched liquid penetrated into the solid more than 1 cm in the middle section of the sample, some small isolated quenched liquid islands were also observed in the solid region up to 2 cm away from the dendritic tips (fig. 23). This was an indication of the extreme case of mushy solidification. The possible eutectic interface behind the dendritic front could not be clearly seen.

During unidirectional solidification, fluid flow occurs as the result of solutal density convection as well as thermal convection. Fluid flow due to thermal convection can be reduced by placing the S/L interface, in the horizontal plane (e.g. solid-down). Thus, the coolest and densest liquid is always close to the inteface. This creates local constitutional undercooling there which retards growth and promotes the development of a non-planar growth. front. As a consequence of this, the S/L interface becomes markedly cellular. The Zn-27% Al is a good example for this case.

In general, the quenched interface morphologies of the commercial

alloys showed almost the same features as those of the pure binary alloys (see fig. 24). Figure 24c indicates the quenched interface of the ZA-27 (commercial) alloy which has the same feature as the Zn-27% Al alloy (fig. 23a). The mushy zone lengths are almost equal for both the binary and commercial alloys, however, the presence of more impurity led to more obvious cellular break-down in the eutectic structure (see figs. 22b).

Solid-Up Specimens

Unlike the solid-down case, the S/L interface was planar even in the Zn-27% Al alloy (see fig. 23a and c). In the Zn-8% Al and Zn-11% Al alloys, the interface proceeded with a planar dendritic tip front and the eutectic front stayed behind it. The eutectic interface became more planar, although it was still cellular. The most pronounced improvement occurred in the Zn-27% Al alloy.

At very large temperature gradients, the dendritic tips indicated a sharp front (fig. 23c). Another common feature of the interfaces for this case was that necking occurred in the quenched-melt just ahead of the interface. This probably happened due to the solidification shrinkage first of the bulk liquid as it entered the quenching medium and froze before the liquid closer to the interface. In the Zn-27% Al alloy, solidification shrinkage behind the dendritic front was seen because of the prior freezing of the liquid ahead of the interface.

During solid-up growth, both thermal and solutal convection occur simultaneously. The densest liquid rises in the cooler region which is close to the S/L interface. This liquid zone is also rich in Zn. It is then carried away from the growing interface by the thermo-solutal convection under the influence of gravity. The interdendritic liquid flows

out from the mushy zone and is also swept away by the convection currents. This makes the S/L interface more planar both on a macroscopic and microscopic scale.

The commercial alloys had almost the same features, the only difference being the more obvious cellulur break-down in the eutectic interface.

3.2 Casting Simulation

As reported in earlier sections, a series of unidirectional freezing experiments have been carried-out with the direction of freezing being vertically upward (solid-down case), vertically downward (solid-up case) and horizontally. These experiments were performed to determine the segregation and microstructural patterns occuring when vertical and horizontal rods froze independently. However, in a real casting, these rods do not freeze independently. Freezing starts as soon as the hot liquid touches the colder mold surface. This causes a more complicated solidification course during the whole process.

The unidirectional freezing experiments using 5mm and 10mm specimen diameters indicated clearly the effect of gravity-induced fluid flow on the segregation and microstructural patterns. In order to have a better understanding of this effect, unidirectional freezing was induced in 50mm diameter specimens using the Zn-27Al alloy. Fig. 25 summarizes the results of these experiments. It is seen that suitably placed chills will produce a sound casting, whereas their absence may lead to underside shrinkage.

To get a better feel for the influence of the presence of a chill block, thermal analyses were carried-out in the solid-down case "with" and

"without" a chill. The presence of a chill induced a temperature gradient of 25°C/cm in the liquid (see fig. 26). This was sufficient to produce sound castings in all the configurations, i.e. no underside shrinkage was observed. The solid-up case shows that relatively little was produced, fig. 25b. This agrees with the unidirectional freezing experiment results (see section 3.1.2.2.). As discussed in the earlier sections, the interdendritic flow of the Zn-rich liquid may be very effective in the solid-down and horizontal growth cases at very small temperature gradients. This causes the separation of the phases which may lead to underside shrinkage.

The information gathered from the various unidirectional freezing experiments may be integrated to provide a description of the topography of the freezing front and in particular the limits of the mushy zone as viewed from the inside of a casting. This is given in Section 3.6.

3.3 Mechanical Properties of Directionally-Solidified Alloys

An attempt was made to determine the mechanical properties of the directionally solidified alloys. As noted earlier, due to experimental difficulties, only a limited number of tests were performed. Because of this, only general comments on the results are appropriate. However, it seems that directional solidification improves the mechanical properties, especially compressive strength (see Table 5-6). This is likely due to the alignment of the Al-rich primaries and the lamellar eutectic phases along the sample axis. However, the sand-cast alloys were also stronger under compression than tension (see Table 7). This suggests that the Zn-Al alloys, in general, show higher compressive strength. This was observed

also in some of the Zn die casting alloys [23].

The SEM micrograph from the fracture surface of the Zn-11%Al alloy shows ductile fracture in the primary dendrite while brittle fractue in the eutectic matrix (see fig. 27).

3.4 Additions of Grain Refiners

Ti, Zr, B, and (Ti + B) are employed as grain-refiners in aluminum alloys to reduce the grain size. By the same analogy, some researchers [7, 13-15] used these elements to refine the primary Al-rich dendrites in the Zn-Al alloys. The effectiveness of these grain refiners was evaluated. Additions in the range of 0.02 - 0.065 wt% were made to the commercial alloys (i.e. ZA-12, and ZA-27). The ZA-8 alloy was not considered because it did not have the commercial importance of the others. Small ingots with the additions were cast into both brass chill and green sand molds. Some of the chill bars were then grown vertically upwards and downwards at a growth rate of 5×10^{-3} cm/sec.

3.4.1. The Effect of Ti

Pollard, et al [13-14] claimed that an addition of not less than 0.04 wt% Ti to Zn-Al alloys containing 7 to 24 wt% Al was sufficient for complete grain-refinement of the primary (Al-rich) phase. The results obtained were in agreement with Pollard's work.

In the ZA-12 alloy, the dendritic pattern disappeared completely in the sand cast structures (see figs. 28-29). In cross-section the primary dendrites became either of a rosette type or took on a more complex rounded

shape. In the chill-cast structure, the dendritic pattern still existed on a finer scale. Large Ti-rich intermetallic compound particles precipitated out in the case of 0.065 wt% Ti.

In the ZA-27 alloy, the dendritic pattern existed in both the sand and chill structures. However, dendrites grew equally in all directions. The primary phase appeared to be more rounded and coarse (see figs. 30-31).

SEM studies on the deep etched samples were also performed in order to identify the nucleating particles. In the refined structure, the primary grains contained the Al_5Ti_2Zn particles as nuclei [13-14] (see fig. 32). That was confirmed with EDS-X-ray analyses in the SEM.

Although Ti seemed to alter the microstructure, there was no improvement in the mechanical properties of the alloys, as expected [7,15].

3.4.2 The Effect of Zr

In the ZA-12 alloy, the dendritic pattern did not disappear completely, but those dendrites which existed in the microstructures grew equally in all directions in the sand structures (see fig. 33). Zr (in the range of 0.02 - 0.065wt %), as a grain refiner, did not seem to be as effective as Ti. In the chill-cast structure, large Zr-rich intermetallic compound particles precipitated-out in the range of 0.05 - 0.065 wt% of Zr. In general, very fine microstructures were obtained. The primary phase lost its dendritic morphology and became globular with the addition of 0.05 wt% of Zr. This has been verified by repeating the experiments several times. The structures obtained were always of an idealized non-dendritic morphology (figs. 33b and d). The reason for this is not well-understood,

but cooling rate may have a critical effect. The extent to which the apparently discrete aluminum "grains" are interconnected could be determined by a more extensive S.E.M. study. The limited work carried-out here would suggest little interconnection exists i.e. they are "globular" primaries.

In the ZA-27 alloy, it appeared that Zr additions affected the primary dendrites (see fig. 34). The sand cast structures looked very similar to the Ti-modified ones. However, the chill cast structure contained more equiaxed dendrites than the Ti-modified ones did.

It is clear that Zr is a grain-refiner but, as noted earlier this did not improve the tensile properties. This might be due to casting defects in the specimens, but this point has not been clearly defined [15].

3.4.3 The Effect of Ti + B

It has been generally found that additions of the ternary Al-Ti-B master alloys to aluminum alloys are more effective grain refiners than the binary Al-Ti master alloys at all addition rates [24]. By analogy, Ti + B (in the form of Al-5Ti-1B master alloy) were added to the ZA-27 alloy. The additions were nominally 0.065 wt% of Ti and 0.013 wt% of B.

As far as the modified structure was concerned, obvious improvements in both the sand and chill-cast structures were obtained (see fig. 35 and 36). Skenazi, et al [15] observed that additions of (Ti + B) not only affected the microstructure but also improved the mechanical properties of the permanent-mold-cast alloys. The addition of both Ti and B resulted in a slight increase in strength while maintaining high ductility (up to 20% elongation). They concluded that this might be attributed to a grain

refining mechanism, but they noted that the eutectoid phase in the modified alloys appeared to be more lamellar [15] and so might play some role in improving the mechanical properties.

3.4.4 Directionally Solidified Alloys with the Additions of Ti and Zr

The chill bars containing 0.05 wt% of Ti and Zr were grown vertically upwards and downwards at a growth rate of 5×10^{-3} cm/sec by employing an air-quench bath.

Any effect of the additions of Ti or Zr on the microstructure could hardly be seen in both the ZA-12 and ZA-27 alloys. This is to be expected because grain-refinement is described [25] to be the result of the nucleation and growth of "new" crystals, i.e. there must be some restriction on the growth of any crystal from the melt. In directional solidification, increased nucleation is eliminated, i.e. nucleation is arranged to occur at one end of the crucible and growth takes place under almost steady state conditions. Thus little change in microstructure would be expected to occur.

3.5 Electromagnetic Stirring (EMS)

The Zn-27% Al alloy was electromagentically stirred under various conditions, since it is the most commercially important alloy and is extremely vulnerable to inverted pipe formation (underside shrinkage).

The application of external energy during solidification disturbs or disrupts the S/L interface, thus the solidification mechanism is changed.

Although cavitation may be responsible for grain refinement in some experimental conditions, it is generally accepted that the best and cheapest method of grain refinement using external energy is to promote crystal multiplication during solidification process. The multiplication mechanism has been attributed to a change in the fluid flow conditions ahead of the S/L interface.

Forced flow of the liquid during solidification is known to play a major role in the formation of the grain structure of cast products. Although the mechanisms of the grain refinement are not thoroughly understood, it is clear that the forced flow can act in several ways, for instance, by eliminating the initial superheat and by providing nuclei for equiaxed grains. This would be expected to induce an early transition from the columnar to the equiaxed structure. Moreover, it is well established that natural convection can also be very effective in large casting and even in small laboratory ingots and produce the same effects [26]. In contrast, it has been shown that when the natural fluid flow is hindered in an ingot, a fully columnar grain structure results [27]. Another effect of forced molten metal flow during solidification is a reduction in macrosegregation which is our concern for this particular case.

3.5.1 Small-Size Ingot (3 lb) in Sand Molds

Initially, the Zn-27% Al alloy was cast into green sand molds without an applied magnetic field. The casting did not show macro-shrinkage at the bottom (fig. 37). This was a good demonstration of the effect of cooling rate on inverted pipe formation, i.e. at a large enough solidification rate, insufficient time is available for appreciable

segregation to occur, therefore an inverted pipe may not form.

The same experiment was repeated in the stirrer with the magnetomotive forces (MMF) directed downwards. Magnetic stirring was applied from the instant of pouring (at 600°C) until the temperature in the ingot had decreased to the eutectic temperature (382°C). As a result, a large cavity was created at the base (fig. 37).

3.5.2 Small-Size Ingots (3 lb) in Heated Ceramic Molds

Since no inverted pipe was observed in the ingot from the sand mold, when cast with no magnetic field, a heated ceramic mold (600°C) was used to provide a longer solidification time, (fig. 38). In specimen (A), the usual underside shrinkage was observed. Then, in specimen (B) in which the MMF was directed vertically downwards, an even larger cavity was seen. In view of this the MMF was reversed so that it was vertically upwards. As a result of this, ingot (C) was obtained without any inverted pipe. This was a very encouraging result, which proved that EMS could eliminate underside shrinkage even in very slow freezing conditions (fig. 38). This is presumed to result from the fact that the perculation of zinc-rich liquid down through the dendritic mesh is hindered. However, a full explanation must await a more detailed study of the resulting fluid flow.

3.5.3 Large Ingots (8 1/2 lb) in Shell Molds

After achieving some success in producing sound casting even at very small solidification rates, the alloy was poured at 600°C into room temperature shell molds with a capacity of 8 1/2 lbs. The results for these experiments were:

i) No stirring; a large cavity was seen.

ii) The stirring was applied immediately after pouring down to eutectic temperature; the cavity was moved above the middle section of the casting.

iii) The stirrer was switched on 30°C below the equilibrium liquidus (≈ 453°C); the cavity, relatively small size as compared to unstirred case, appeared at the bottom.

iv) As for (iii) with the magnetic field on 10°C above liquidus (≈ 495°C); no cavity was observed, except very small defects under the side surface.

v) As for (iii) with stirrer on 10°C below the liquidus (≈ 475°C). the reduced size cavity appeared once again (see fig. 39).

As a conclusion of these three sets of experiments, it may be stated that EMS eliminated the underside shrinkage and produced relatively sound castings when the stirrer was on throughout the whole solidification range and the MMF was upwards.

Unfortunately, there is no information about the actual flow pattern created in the melt by the MMF and so it is not possible to discuss the results in more detail. In spite of this, some speculations can be made by considering the idealized flow pattern. In the case of MMF downward, the natural convection is enchanced at the beginning, of solidification and probably promotes an early transition from a columnar to an equiaxed structure. When the fraction of solid in the melt reaches a certain level, the bulk liquid motion is stopped. Liquid transport can then occur only through the interdendritic channels. The Zn-rich interdendritic liquid already has a tendency to flow down through the channels and settles down

at the bottom of the casting. A downwards MMF pushes the heavier liquid down and enchances the separation. Presumably, the formation of a cavity in the sand mold ingot and a larger pipe in the ceramic mold ingot maybe explained by considering the heating effect of EMS which reduces the cooling rate and the enhances the interdendritic fluid motion. In contrast, upward MMF hinders the natural convection and may stabilize the columnar growth; In addition it may inhibit the interdendritic fluid flow which is believed to be the predominant factor in producing macrosegregation in these castings [21].

3.5.4 Chemical Analyses and Metallographic Studies on the Unstirred and Stirred Ingots.

In order to determine the effects of stirring on both the microstructure and the composition variation throughout the ingot, chemical analyses and a metallographic study were also performed. The chemical analysis results showed that EMS produced a relatively uniform chemical composition throughout the ingot (see fig. 40 and Table 8).

Figure 41 indicates the difference in the amount of interdendritic liquid at the top and the bottom of the unstirred ingot. It was quite clear that the Zn-rich liquid segregated towards the bottom while the primary dendrites floated to the top of the ingot. In the stirred ingot, the microstructure appeared to be relatively uniform (see fig. 42). However, in some regions, the liquid was trapped between the primaries. The small pockets of liquid solidified thereby leaving shrinkage due to the volume change upon freezing.

In order the check whether EMS produced a really sound casting or

distributed the shrinkage porosity throughout the casting, density measurements on the stirred ingot were done. The density of the ZA-27 (commercial alloy which contains Cu and Mg) alloy is 5 g/cm^3 [23]. The measured density was 4.85 g/cm^3 which was very close to the given value within the experimental error. This once again proved that EMS produced a sound casting with uniform chemical composition but with some distributed porosity.

3.6 Development of Underside Shrinkage in Sand Castings

Whilst all the Zn-Al alloys tend to display some underside shrinkage, it is possible to eliminate the problem in the case of ZA-8 and ZA-11 alloys by adjusting such casting variables as pouring temperature, mold type and riser volume and placement. However, underside shrinkage is far more severe in the ZA-27 alloys, and may only be removed, by using large temperature gradients in the liquid (Section 3.2., fig. 25) or magnetic stirring (Section 3.5, fig. 39).

That there is likely to be a severe segregation problem in the Zn-27% alloy may be judged from an inspection of the Zn-Al binary phase diagram, fig. 1. The first solid to appear as the alloy liquid cools will be dendrites of approximately 60% Al. These will form at the cooler surfaces of melt and reject zinc into the adjoining liquid. In a simple short cylinder casting losing heat from all surfaces, as in a sand casting, the aluminum dendrites will form the outer skin. As they grow, the more dense zinc-rich liquid between the dendrite stems and arms will tend to "percolate" through the aluminum "forest" towards the lower regions of the

free liquid in the casting. The manner in which this takes place is not well described but the transparent analogue work done to simulate freckle formation in unidirectionally-grown gas turbine blades suggests that it could well be relatively coordinated (28). If the bottom surface chilling is not significant, dendrite detachment may ensue and, with accompanying inverse segregation, may lead to the continuing existence of a zinc-rich liquid layer at the base of the casting. Since the zinc-rich layer contains an appreciable aluminum content, oxidation will take place to form an outer coating of alumina. Then, as solidification proceeds, the volume contraction accompanying solidification places the remaining liquid in tension. Some distributed porosity results but, in the main, this constraint is relieved by the external (ambient) pressure "pushing" on the alumina film and the adjoining liquid to force it up into the body of the casting to give the characteristic inverted pipe.

This was the generalised view of underside shrinkage formation by the Principal Investigator at the beginning of this study. Little detailed quantitative data concerning the fluid flow and segregation likely to occur in various casting geometries was available. However, as the result of the work carried-out, a closer description of the freezing of a chunky Zn-27% Al casting may now be given.

Consider first a roughly equiaxed casting ABCD fig. 43 and assume that there is relatively little coordinated fluid flow through any primary dendrite "forest" at the ingot perimeter faces. The details of the nature of the solidification fronts should be obtainable from the unidirectional freezing of "liquid cores" at sites 1,2,3 and 4, through the left, top, right and bottom faces of the casting respectively. The freezing of relatively narrow cores are reported in Section 3.1 and the influence of

scale in the selection of the diameter of the core is discussed in Section 3.2. The information gathered from these various unidirectional freezing experiments may be integrated to provide a description of the topography of freezing front and, in particular, the limits of the mushy region as viewed from the inside after casting. It is clear that the separation of the tips of the aluminum-rich dendrites from the the eutectic front is a function of the local temperature gradient in the liquid. For a given superheat and mold-type, it is expected that the local temperature gradient will be greater at Site 2, than at Sites 1 and 3, fig. 43. Similarly, that at Site 4 will be appreciably smaller than even those at Sites 1 and 3. In addition, the quenched and decanted interfaces showed that the dendrite tips at Site 1 (and Site 3) were coplanar and likely to be parallel to the eutectic freezing surface. However, both planes would be inclined somewhat towards the vertical centre-line. In addition because of the fluid flow, the dendrite stems would be inclined to meet the falling liquid.

At the top, Site 2, a larger value of G will decrease the thickness of the mushy-zone but the dendrite tip front is unlikely to be planar because of the coordinated flow of denser zinc-rich fluid in near-vertical channels through the dendrite mesh, as noted by Copley et al (28) in their transparent analogue for solid-down growth with freckle formation.

At the bottom of the casting, the eutectic front is well behind the ragged mushy dendrite front and in some areas may not be present since, as soon as the skin of the upper part of the casting becomes rigid, underside shrinkage will begin. Then, because of the free liquid will tend to flow progressively to the centre of the bottom face, an inverted pipe is able to form as a result of the external ambient pressure.

4. Conclusions

The specific conclusions from the experimental work carried-out are:

1. The microstructure of the horizontally grown alloys resulted in a well-defined segregation pattern. The Zn-rich liquid accumulated in the bottom section of the specimen tube while the top was occupied by the Al-rich primaries.

2. The S/L interface of horizontally-grown alloys was inclined away from the growth direction. The mushy zone lengths of the alloys (Zn-8% Al, Zn-11% Al and Zn-27% Al) were respectively 4.5, 7 and 20 mm at a growth rate of 5×10^{-3} cm/sec with temperature gradient of 10°C/cm.

3. Decanting experiments confirmed these facts as a result of observations on the bottom surfaces of the samples.

4. The macrosegregation pattern seemed to be independent of the tube diameter for those diameters studied, 5 to 10 mm.

5. In solid-down growth case, the S/L interfaces showed a non-planar morphology in a macroscopic scale, dendritic tip front was ragged, especially in the Zn-27% Al alloy. In the Zn-8% Al and Zn-11% Al alloys the cellular eutectic interface was observed behind the dendritic front.

6. Unlike the solid-down growth, the S/L interface in solid-up growth advanced with a planar front. This improvement was more obvious in the Zn-27% Al alloy.

7. The commercial alloys indicated almost the same behaviour as the pure binary alloys did, except the degree of fineness in the microstructure.

8. Although additions of Zr, and Ti affected both the sand and chill cast structure of the ZA-12 and ZA-27 alloys, Ti-B additions appeared to be

more effective in refining the structure.

9. EMS eliminated most of the macrosegregation and produced a relatively sound casting when the MMF was vertically upwards and applied during the whole solidification range.

10. Metallographic studies and chemical analyses proved that EMS was effective. The density measurements on the whole stirred casting also proved that the casting was sound containing only microshrinkage.

11. Directional solidification improved the compressive yield strength.

These specific conclusions may be generalised to describe the freezing of a simple "chunky" casting as follows:

12. Interdendritic fluid flow leads to the formation of underside shrinkage in Zn-Al alloys.

13. The boundaries of the mushy region of the vertical walls of all Zn-Al casting are probably well-defined and inclined to the centre of the casting.

14. The boundaries of the mushy region on the horizontal surfaces of a Zn-27% Al casting are more ragged, particularly that of the bottom surface.

15. A temperature gradient of 25°C/cm in the liquid at the solid/liquid interface of a Zn-27% Al casting will ensure the absence of an inverted pipe.

16. Electro-magnetic stirring may be used to aggravate or remove inverted pipe formation in small castings.

References

1. Roudtke, S.F., "New Zn Die Casting Alloys and Their Applications" Transactions of the 6th SDCE International Die Casting Congress, Technical Paper No. 104, Cleveland, OH (Nov. 1980).

2. "Design Applications of Gravity Casting Zinc, ILZRO-12", p. 36, Zinc Institute, New York, N.Y. (1972).

3. Pollard, W.A. and Edwards, J.O., Met. Trans. B, 8B (1977), pp. 157-168.

4. Idem, ibid, pp. 597-599.

5. Devillers, L.P., and Niessen, P., Corrosion Science, 16 (1976), pp. 243-252.

6. Gervais, E., Levert, H., and Bess, M., Trans. AFS, 88 (1980), pp. 183-194.

7. Sahoo, M., and Whiting, L.V., Report MRP/PMRL 83-43 (TR), CANMET, Ottawa, Canada (June 1983).

8. Barnhurst, R.J., Gervais, E., and Bayles, F.D., Trans. AFS, 91 (1983), pp. 569-584.

9. Habiby, F. and McNallan, N.J., unpublished work.

10. Yurko, G.A., Whitaker, D.A., and Parr, J.G., CIM Transactions, vol. LXIII, (1960), pp. 436-442.

11. Guttman, H. Internal Report PM-R-59-25; Physical Metallurgy Division, Mines Branch, Department of Mines and Technical Surveys, Ottawa, Canada, 1958.

12. Idem, Internal Report 61-48, Physical Metallurgy Division, Mines Research, Department of Mines and Tech;nical Surveys, Ottawa, Canada, (1961).

13. Pollard, W.A., Pickwick, K.M., Jubb, J.T., and Packwood, P.H., Canadian Metallurgical Quarterly, 13(4), (1974), pp. 535-543.

14. Pollard, W.A., idem, 13(4), (1974), pp. 597-606.

15. Skenazi, A.F., Pelerin, J., Coutsouradis, D., Magnus, B., and Meeus, M., Metall., 37 (1983), pp. 898-902.

16. Sahoo, M., Whiting, L.V., and White, D.W.G., Report MRP/PMRL 84-86 (OP-J), CANMET, Ottawa, Canada, 1984.

17. Chalmers, B., Principles of Solidification, Robert E., Krieger, Malabor, Florida, 1982 (original Ed. 1964).

18. Solidification, ASM, Metals Park, Ohio, 1971.

19. Azouni, M.A., Physicochemical Hydrodynamics, 2(4), (1981), pp. 295-309.

20. Davies, J.D., J. Inst. Metals, 93, (1964/1965), pp. 197-206.

21. Voller, V.R., Moore, J.J., and Shah N.A., Metals Technology, 10 (1983), pp. 81-84.

22. Mollard, F.R. and Flemings, M.C., Trans. TMS AIME, 239 (1967), p. 1534.

23. Enginering Properties of Zinc Alloys, ILZRO, Inc., 292 Madison Avenue, New York, N.Y. 10017, (1981).

24. Davies, I., et al, Met. Trans. A., 1 (1970), pp. 275.

25. Arnberg, L., et al, Solidification Technology in the Foundry and Casthouse Metals Society, (1980).

26. Witzke, S. and Riquet, J.P., Acta Met., 30 (1982), pp. 1917-1922.

27. Uhlmann, D.R., Seward, P.D., and Chalmers, B., Trans. TMS-AIME, 236 (1965) pp. 527-531.

28. S.M. Copley, A.F. Giamei, S.M. Johnson and M.F. Hornbecker, "The Origin of Freckles in Unidirectionally Solidified Castings", Advanced Mater. Res. Dev. Lab. Rept. No. 69-028, Pratt and Whitney Aircraft, Middletown Conn., 1969, p. 19.

Appendix I

Electromagnetic Stirring (EMS)

Forced fluid flow of the liquid influences the formation of the cast structures, thus changing the segregation patterns. The flow must be fast enough to prevent mini-ingot formation and prevent crystal multiplication.

Quantitative characterization of the velocity fields and mixing rates requires the simultaneous solution of the turbulent Navier-Stokes equations along with the equations of magnetohydrodynamics. This is beyond the scope of this thesis.

An attempt is made by giving the force distribution, contour map detailing the transverse profile of the magnetic field strength across the bore of the stirrer, and idealized flow patterns to develop a sense for the actual fluid flow pattern occuring in that particular experimental condition, Figure A1.

Electrical Layout

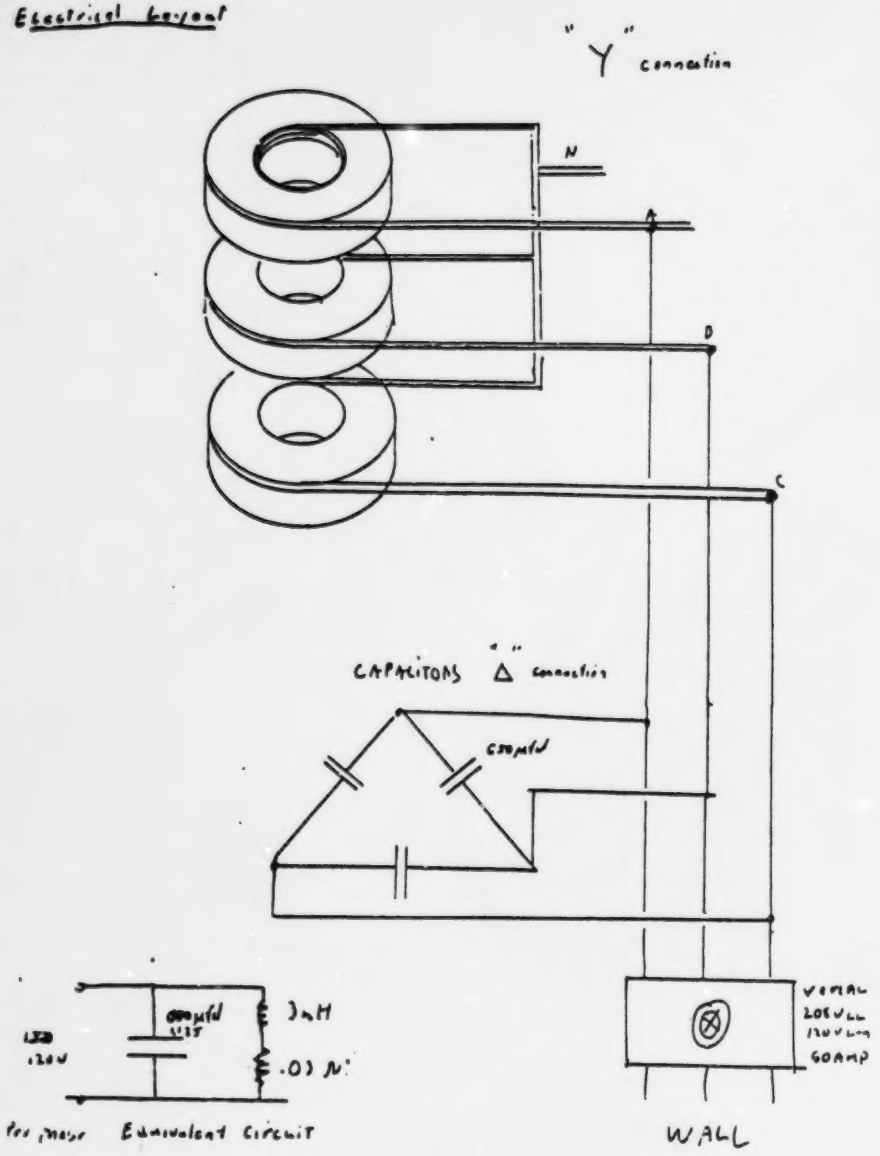

Figure A1

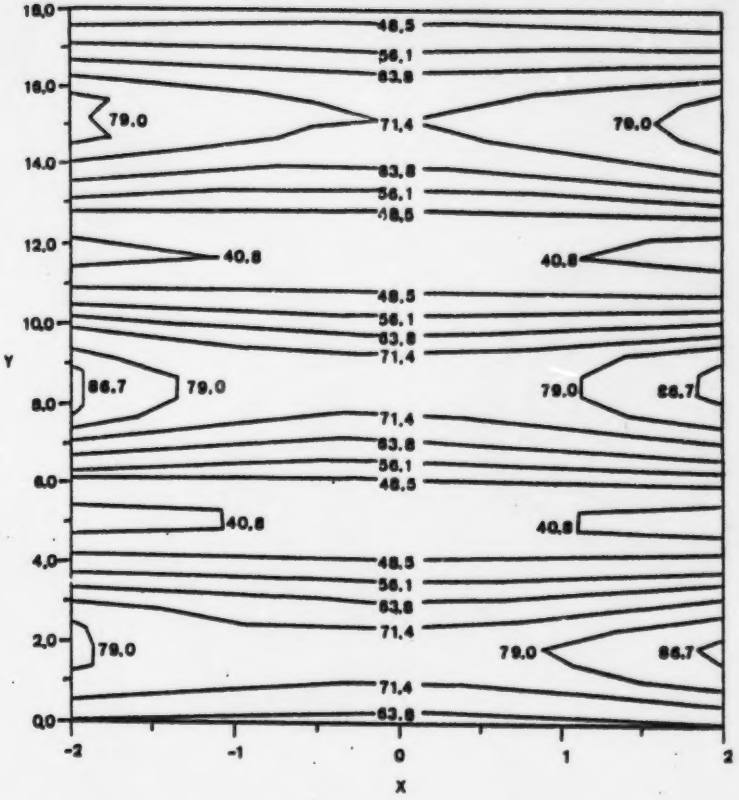

Contour map detailing the transverse profile of magnetic field strength across the bore of the stirrer. Data plotted from flux probe measurements taken with a total machine current of 50.3 amps or 50 percent of full power. Magnetic flux measurements shown in milli-teslas.

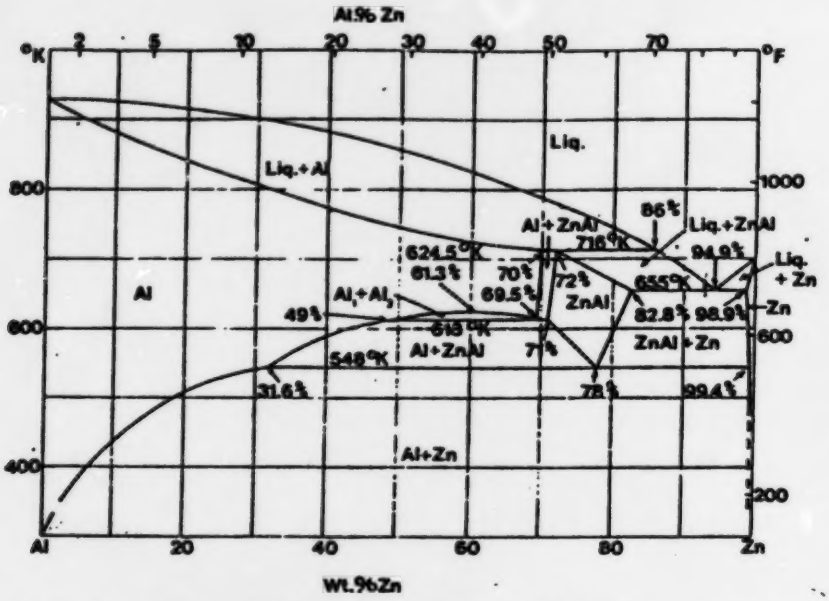

Fig. 1. The binary Zn-Al equilibrium diagram. The first solid to form in the Zn-27%Al alloy is 60%Al.

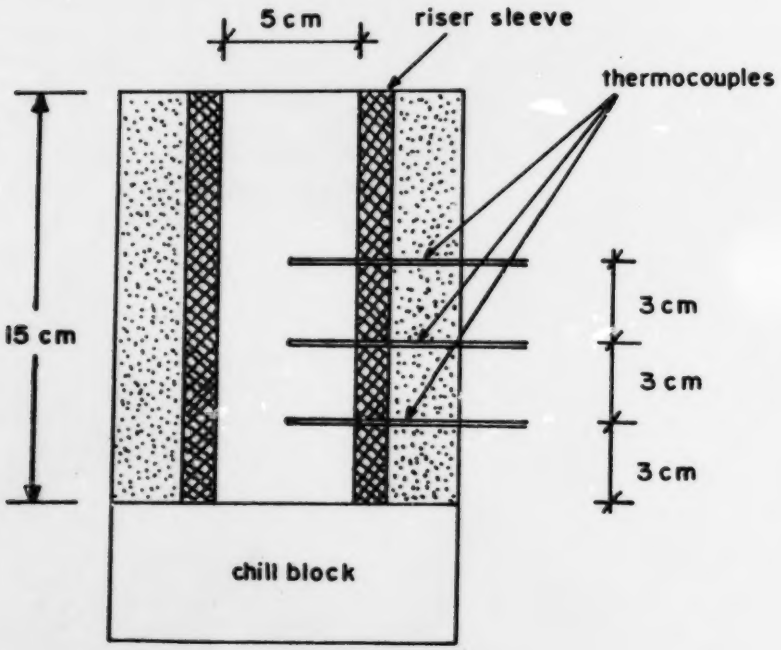

Fig. 2. Schematic representation of the cross-section of a casting (i.e. solid-down case) showing thermocouple positions.

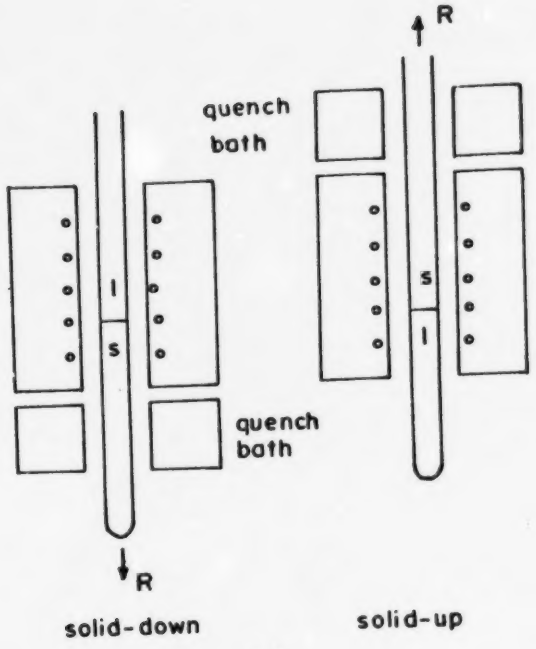

(a)

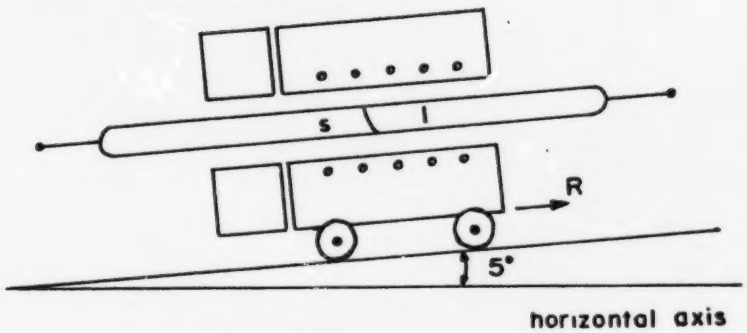

(b)

Fig. 3. Crystal growers (a) vertical; (b) horizontal

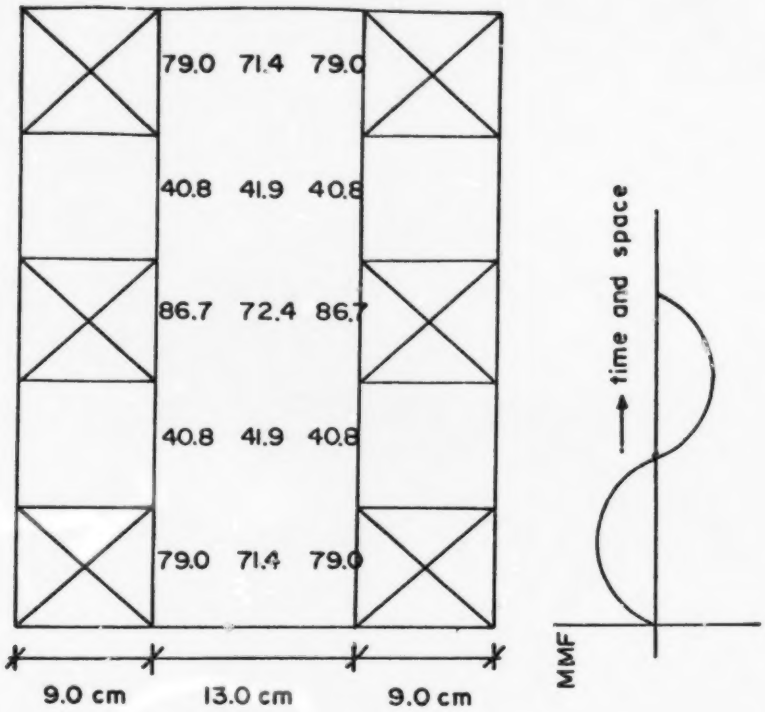

(a)

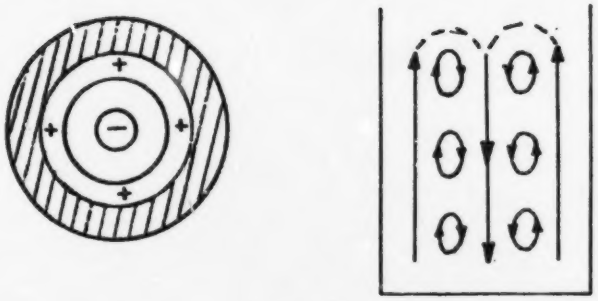

(b) (c)

Fig. 4. (a) Schematic drawing of the mechanical cross-section of the stirrer and field strengths in milli-teslas
(b) Force distribution (end view)
(c) Idealized fluid flow pattern

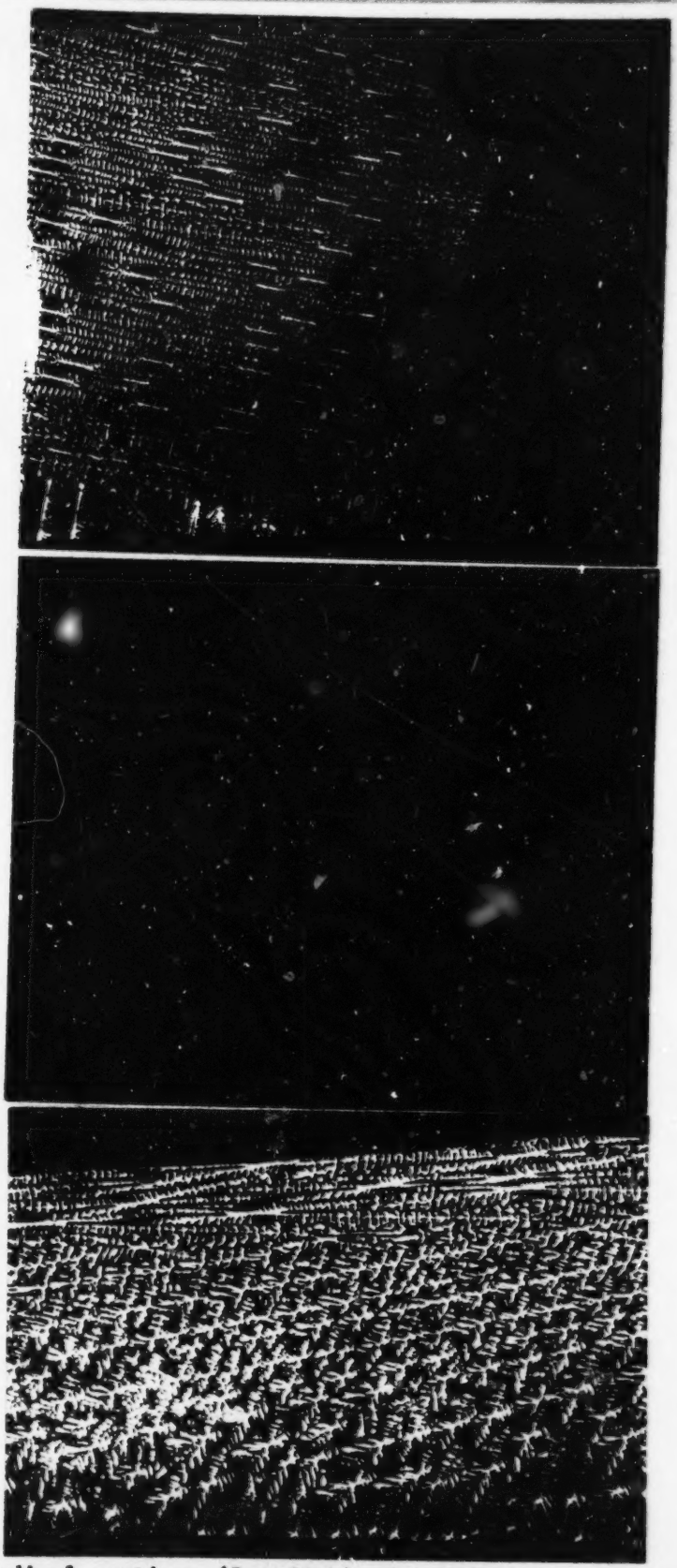

(a)

(b)

Growth
Direction

(c)

Fig. 5. Longitudinal sections (5mm dia.) of horizontally-grown Zn-11%Al alloy, R(growth rate) = 5×10^{-3} cm/sec, G(temperature gradient) = 10°C/cm. (x16)
(a) start-end, (b) central section, (c) finish-end
R = 5×10^{-3} cm/sec., g = 10^{o} c/cm

Growth
Direction

←

(a)

(b)

Fig. 6. Longitudinal sections (5mm dia.) of horizontally-grown alloys (central sections), R = 5 x 10^{-3} cm/sec, and G = 10°C/cm.

(a) Zn-8%Al, (b) Zn-27%Al (x16)

(a)

(b)

Growth
Direction
→

(c)

Fig. 7. Central longitudinal sections of the alloys grown horizontally (10mm dia.), R = 5 x 10^{-3} cm/sec, and G = 10°C/cm.

(a) Zn-8%Al, (b) Zn-11%Al, (c) Zn-27%Al (x6)

Growth Direction

→

Fig. 8. Longitudinal section of the quenched interface of the Zn-27%Al alloy grown horizontally (5mm dia.), $R = 5 \times 10^{-3}$ cm/sec, $G = 10°C/cm$. (x10).

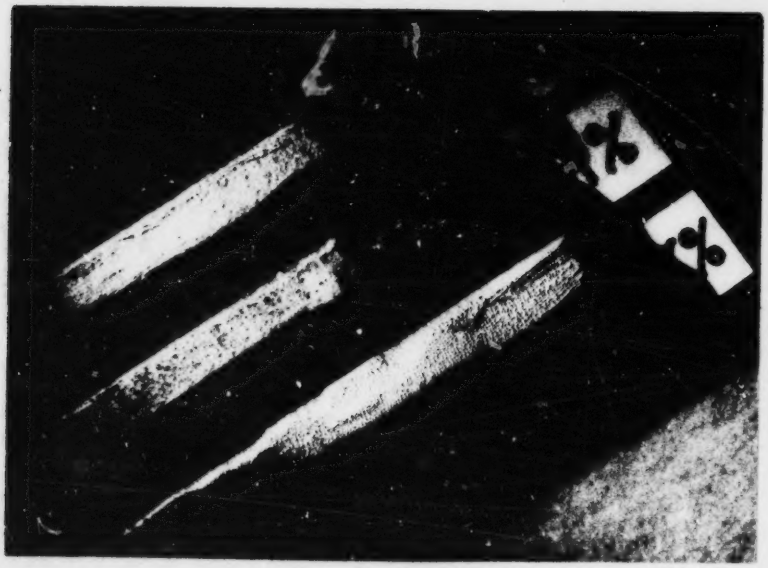

Fig. 9. Bottom surfaces of the decanted alloys grown horizontally $R = 5 \times 10^{-3}$ cm/sec. (x2).

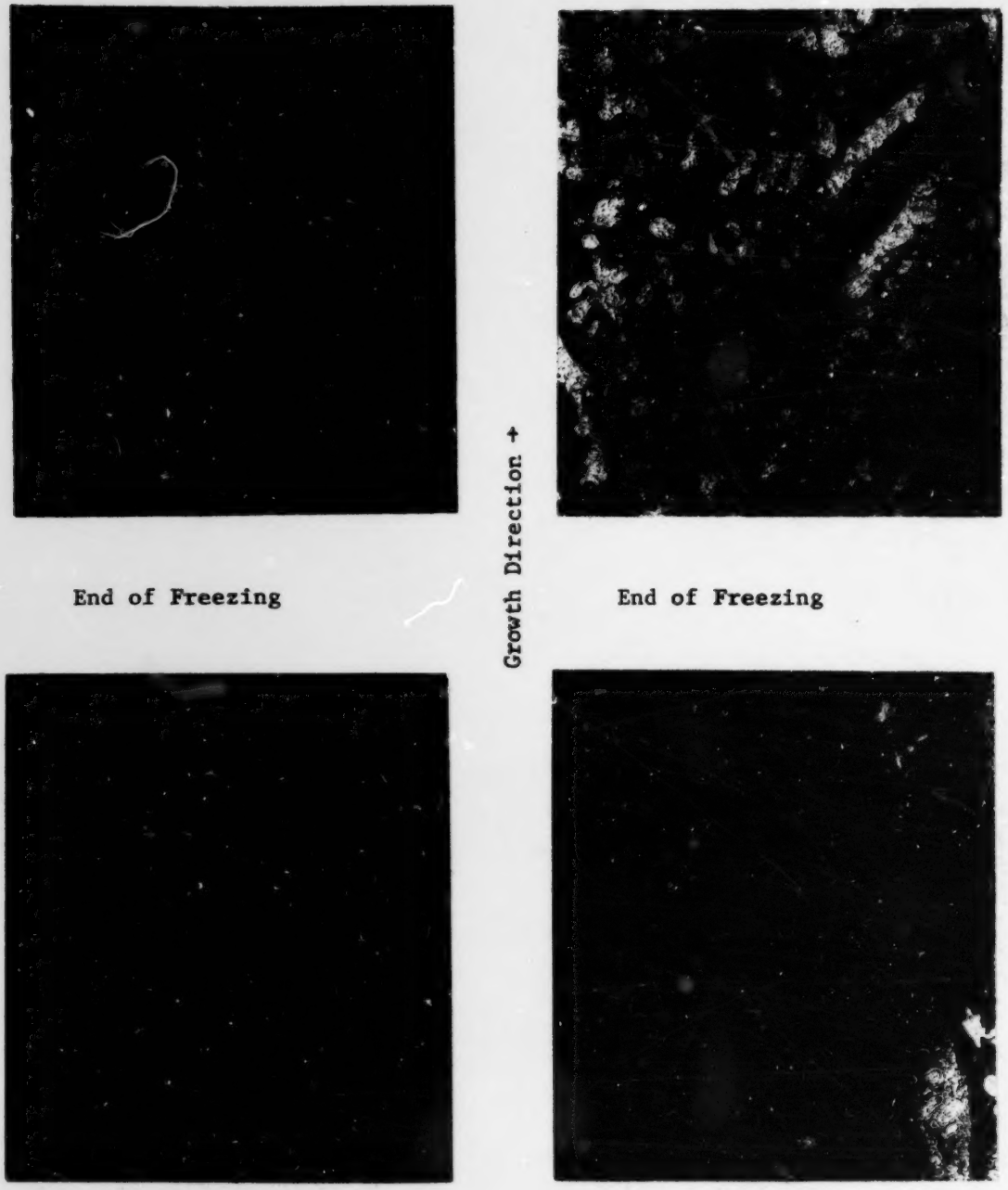

Fig. 10. Microstructures of the Zn-8%Al alloy grown vertically upwards. 5mm dia. (left), 10mm dia. (right), $R = 5 \times 10^{-3}$ cm/sec, $G = 44°C/cm$. (x100).

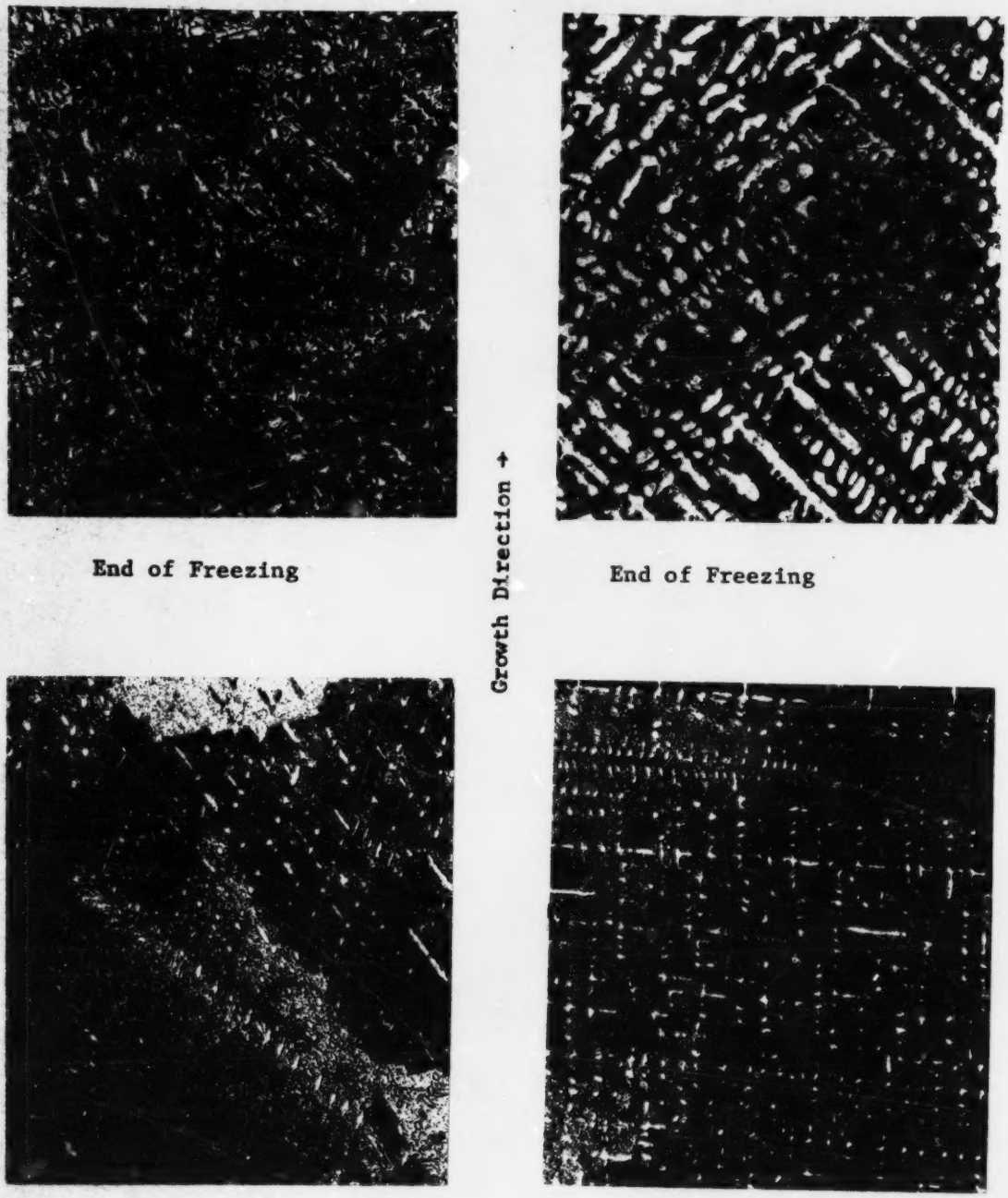

Fig. 11. Microstructures of the Zn-8%Al alloys grown vertically upwards (5mm i.d.),

$R = 10^{-2}$cm/sec, $G = 62°C/cm$ (left)

$R_2 = 10^{-1}$cm/sec, $G_2 = 20°C/cm$ (right). (x100).

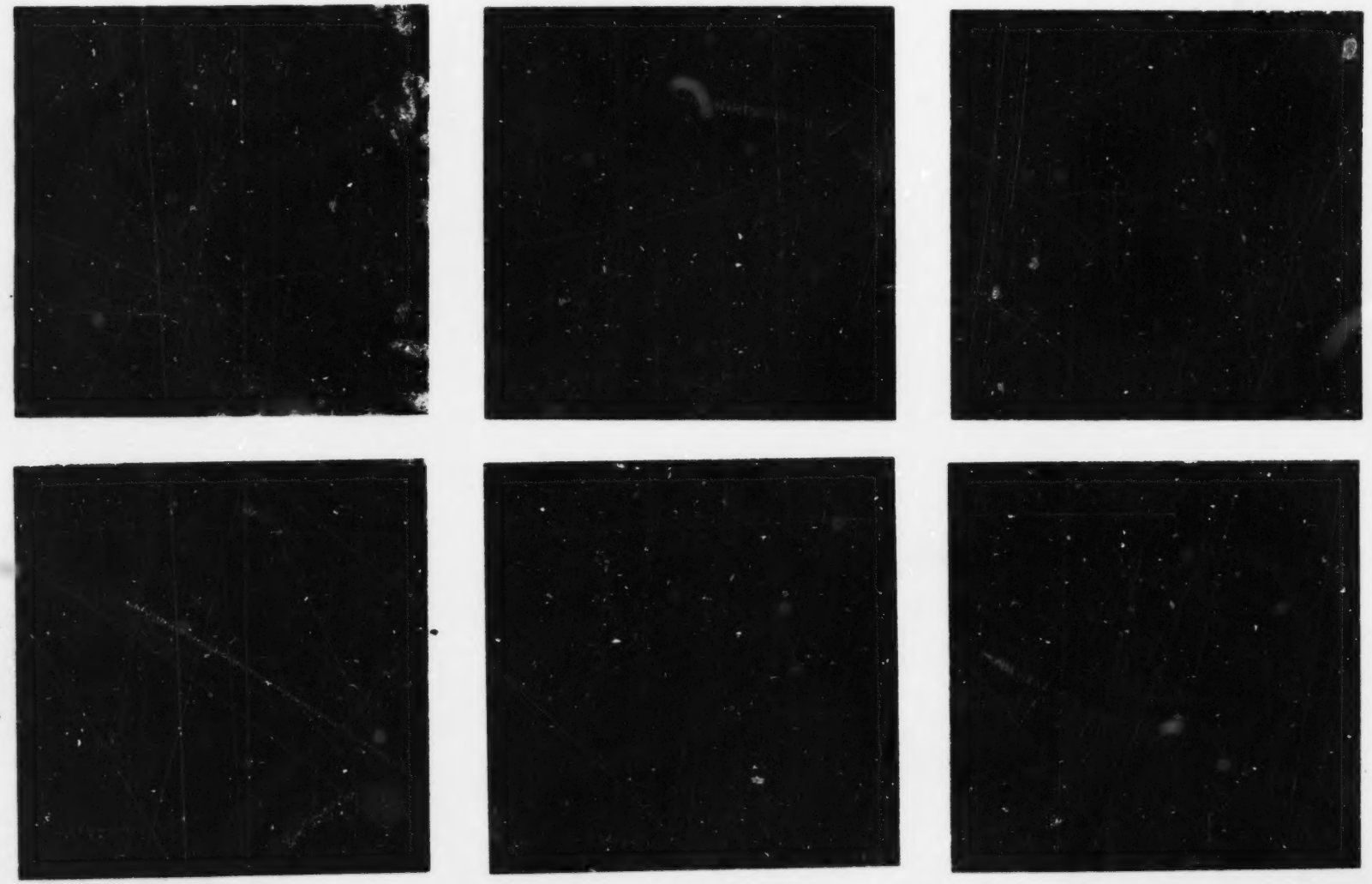

Fig. 12. Microstructures of the Zn-11%Al alloys grown vertically upwards (5mm i.d.).
(a) $R = 10^{-3}$cm/sec, $G = 44^{\circ}$C/cm, (b) $R = 10^{-2}$cm/sec, $G = 62^{\circ}$C/cm,
(c) $R = 10^{-1}$cm/sec, $G = 20^{\circ}$C/cm. (x100).

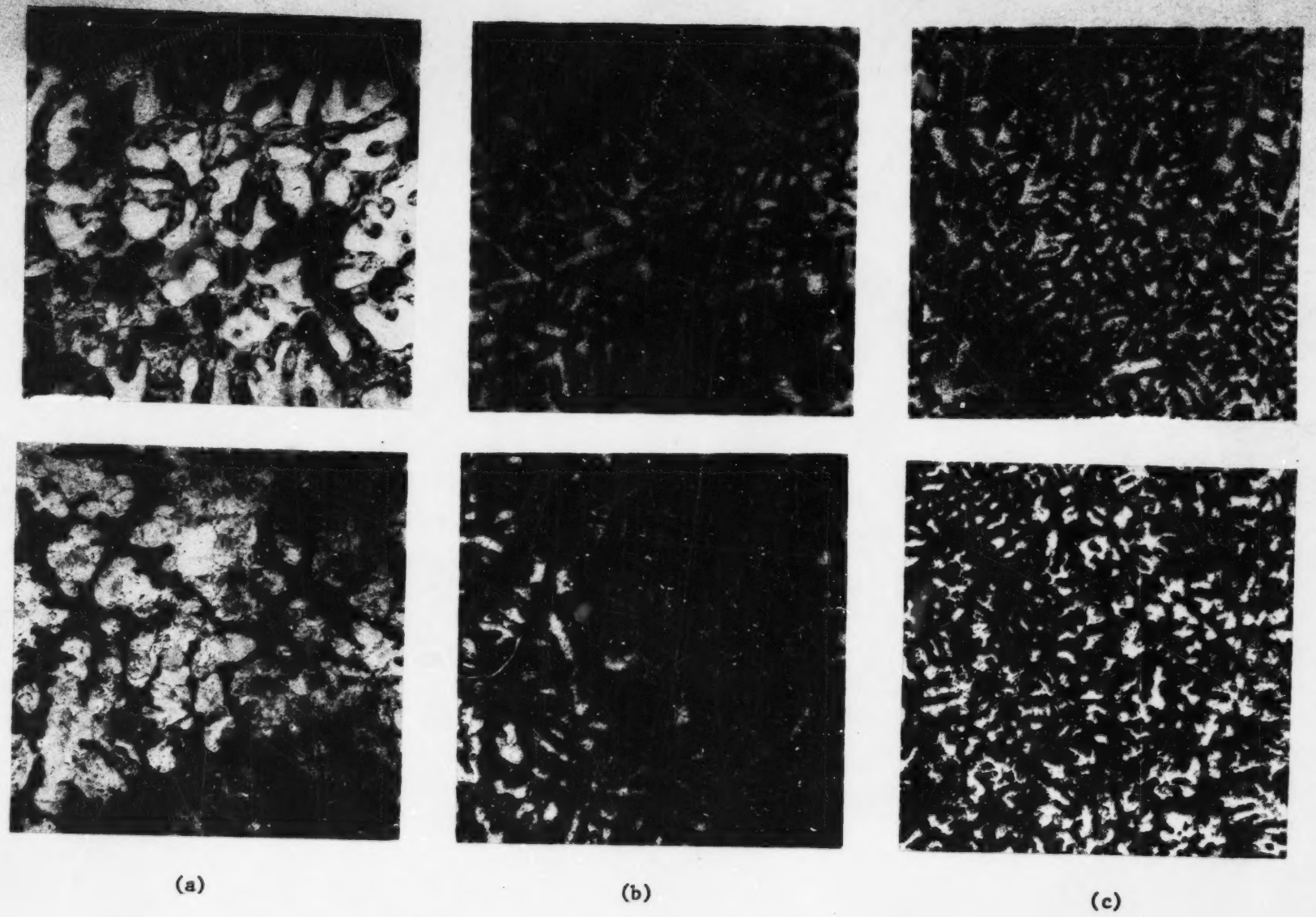

Fig. 13. Microstructures of the Zn-27%Al alloy grown vertically upwards (5mm i.d.).
(a) $R = 10^{-3}$cm/sec, $G = 44^{\circ}$C/cm, (b) $R = 10^{-2}$cm/sec, $G = 62^{\circ}$C/cm,
(c) $R = 10^{-1}$cm/sec, $G = 20^{\circ}$C/cm. (x100).

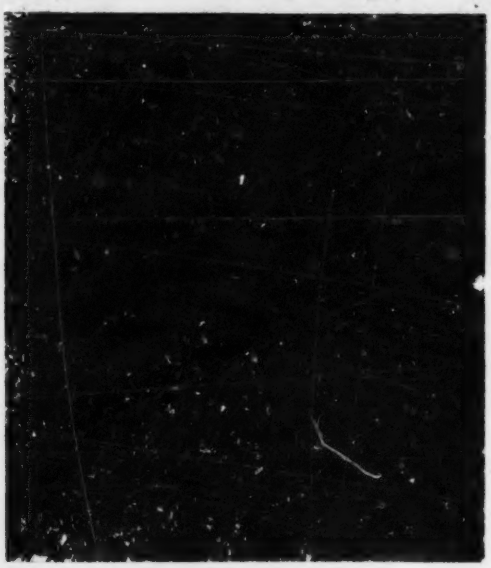

End of Freezing

Growth Direction

Start of Freezing

Growth Direction

Start of Freezing

(a)

End of Freezing

(b)

Fig. 14. Microstructures of the ZA-8 (commercial) alloy, R = 5×10^{-3} cm/sec.

(a) Solid-down, G = 44°C. (b) Solid-down, G = 56°C. (x100).

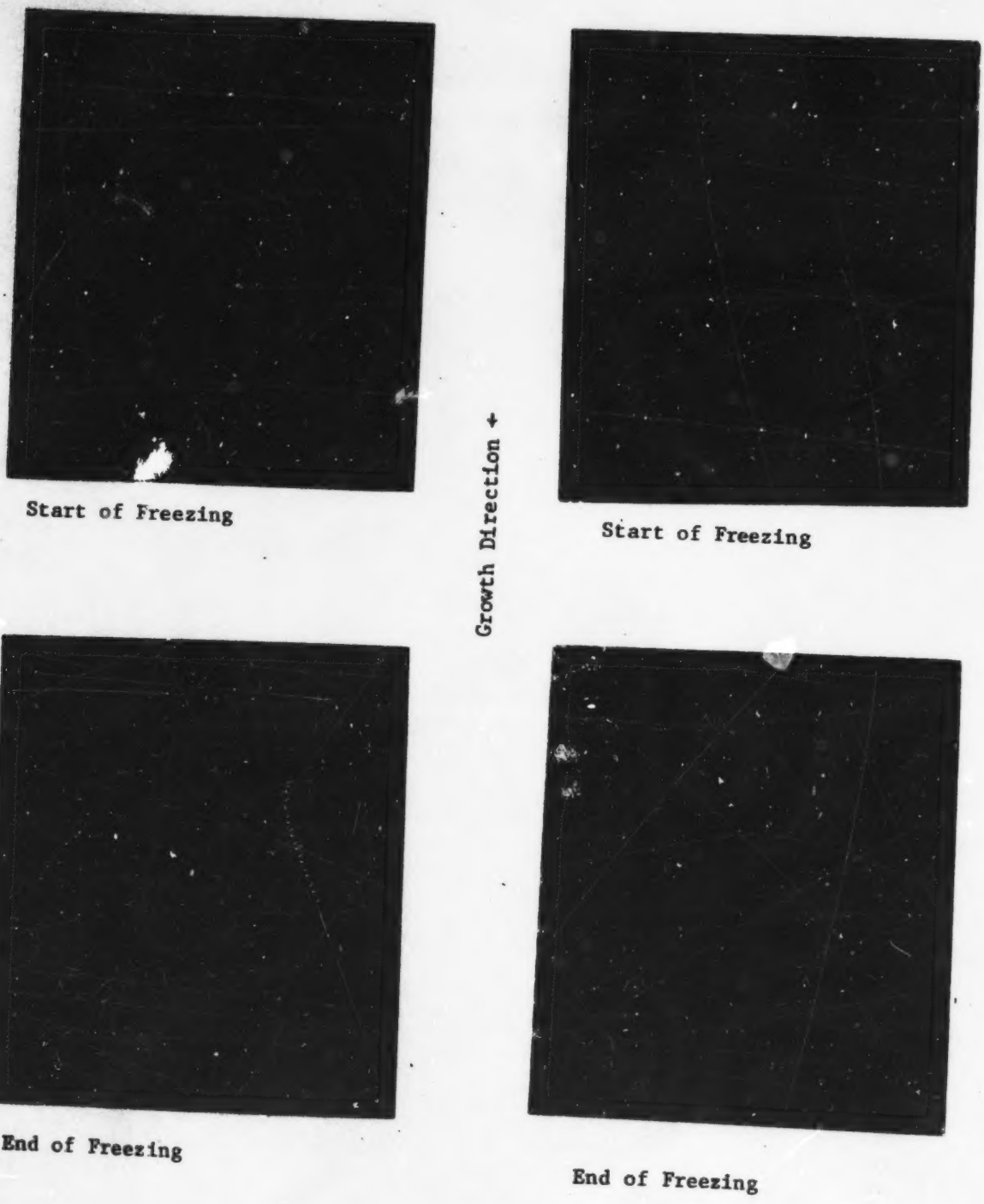

Fig. 15. Microstructures of the Zn-8%Al alloy grown vertically downwards. 5mm i.d. (left), 10mm i.d. (right). $R = 5 \times 10^{-3}$ cm/sec, $G = 56°C/cm$. (x100).

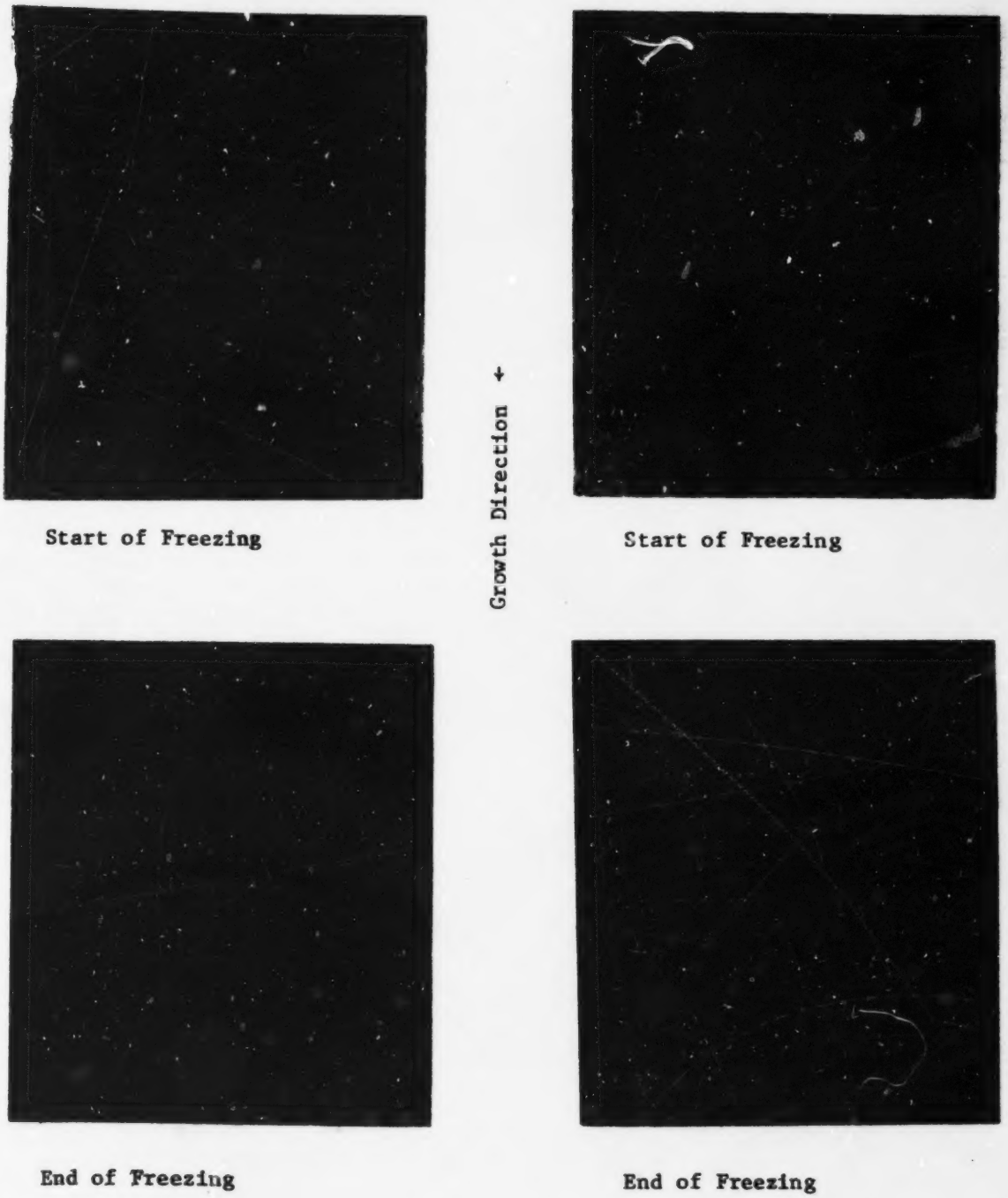

Fig. 16. Microstructures of the Zn-8%Al alloy grown vertically downards (5mm i.d.) left ($R = 10^{-2}$ cm/sec, $G = 62°C$), right ($R = 10^{-1}$ cm/sec, $G = 20°C/cm$. (x100).

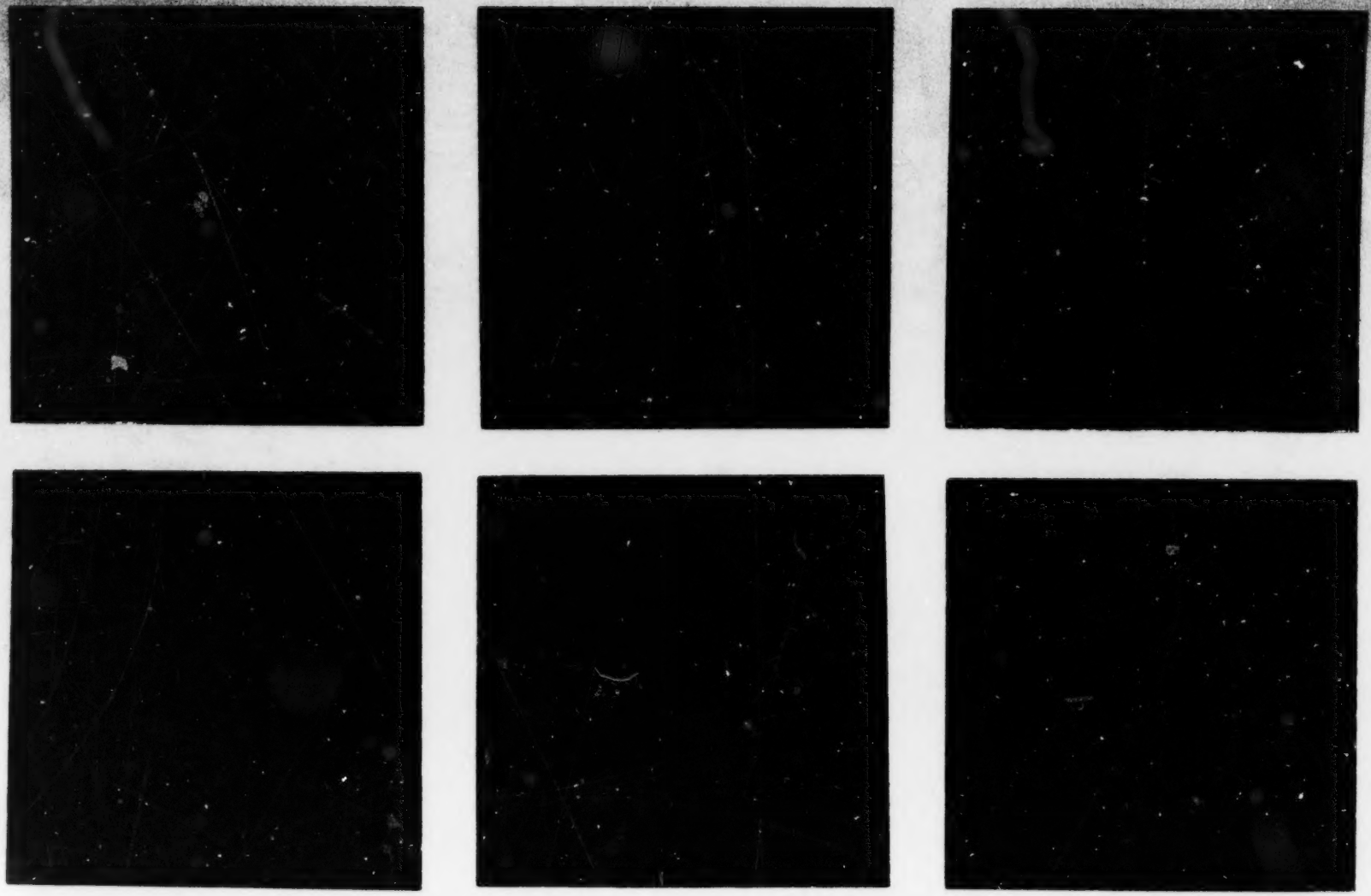

Fig. 17. Microstructures of the Zn-11%Al alloy grown vertically downwards (5mm dia.)

(a) $R = 5 \times 10^{-3}$ cm/sec, $G = 56^{\circ}$C/cm (b) $R = 10^{-2}$ cm/sec, $G = 62^{\circ}$C/cm (c) $R = 10^{-1}$ cm/sec, $G = 20^{\circ}$C/cm. (x100).

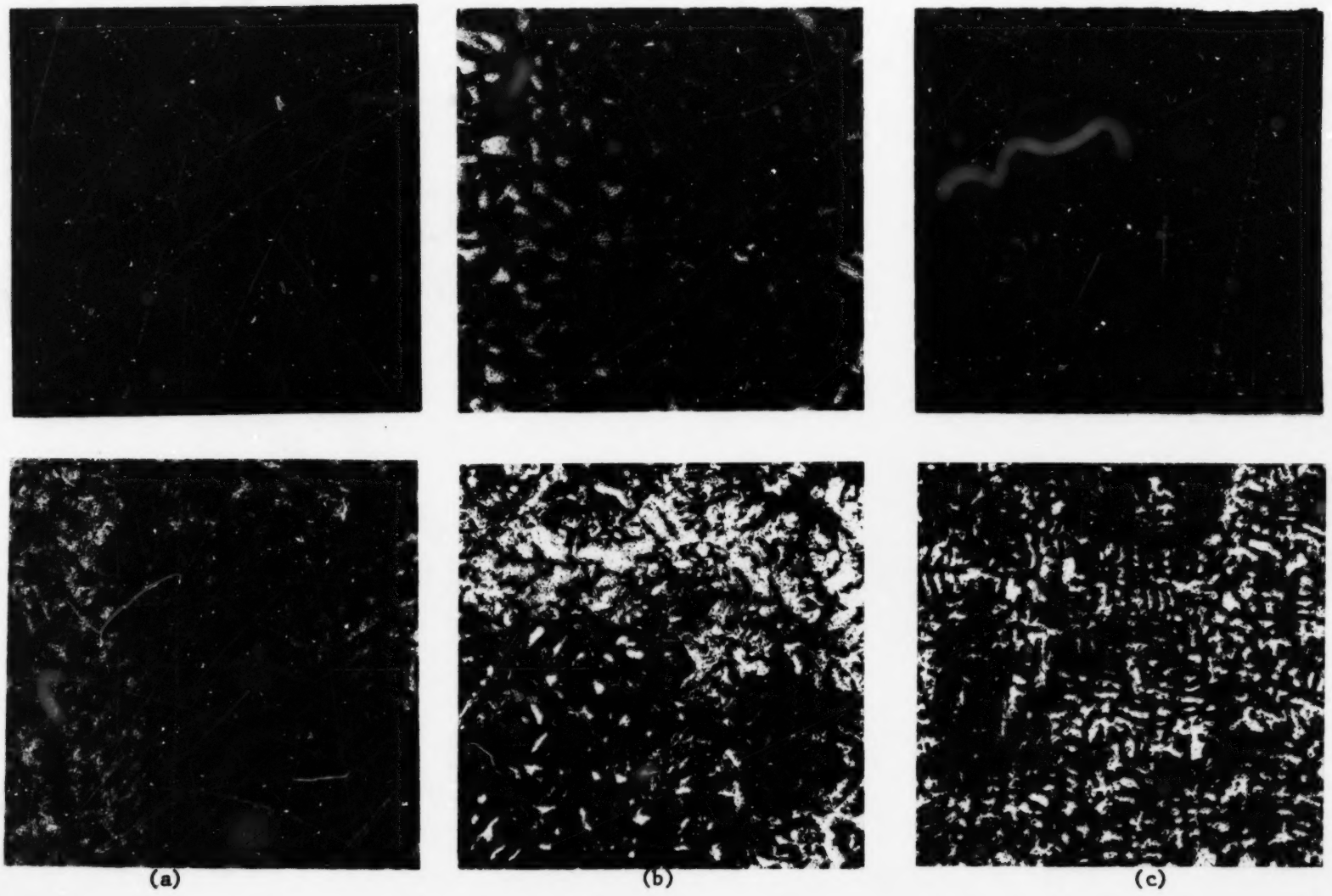

Fig. 18. Microstructures of the Zn-27%Al alloy grown vertically downwards (5mm dia.)

(a) $R = 5 \times 10^{-3}$ cm/sec, $G = 56^{\circ}$C/cm (b) $R = 10^{-2}$ cm/sec, $G = 62^{\circ}$C/cm
(c) $R = 10^{-1}$ cm/sec, $G = 20^{\circ}$C/cm. (x100).

(a) (b) (c)

Fig. 19. Microstructures of the alloys grown vertically downwards (5mm dia).

$R = 5 \times 10^{-1}$ cm/sec, G = 250°C/cm (a) Zn-8%Al, (b) Zn-11%Al, (c) Zn-27%Al. (x100).

Growth Direction

(a)

Growth Direction

(b)

Fig. 20. Longitudinal sections of quenched interfaces of the Zn-8%Al alloys (5mm dia.) $R = 5 \times 10^{-3}$ cm/sec. (a solid-down, G = 44°C/cm (x14) (b) solid-up, G = 56°C (x14).

(a)

Growth Direction

Growth Direction

(b)

Fig. 21. Longitudinal sections of quenched interfaces of the Zn-11%Al alloys (5mm dia.)
$R = 5 \times 10^{-3}$ cm/sec. (a) solid-down, $G = 44°C/cm$
(b) solid-up, $G = 56°C$ (x13).

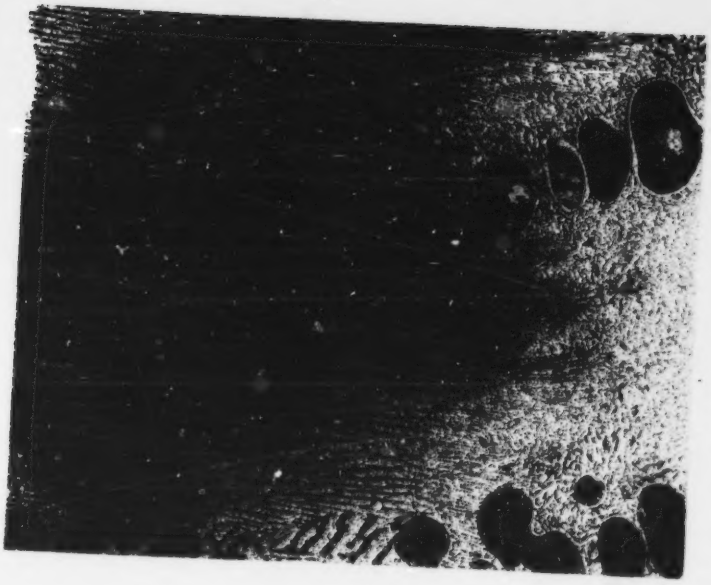

(a)

(b)

Growth Direction →

Fig. 22. Longitudinal sections of quenched eutectic interfaces (5mm dia.) $R = 5 \times 10^{-3}$ cm/sec. (a) Zn-8%Al, solid-up, $G = 56^{\circ}C/cm$. (x400). (b) ZA-8, solid-up, $G = 120^{\circ}C/cm$ (x400).

(a)

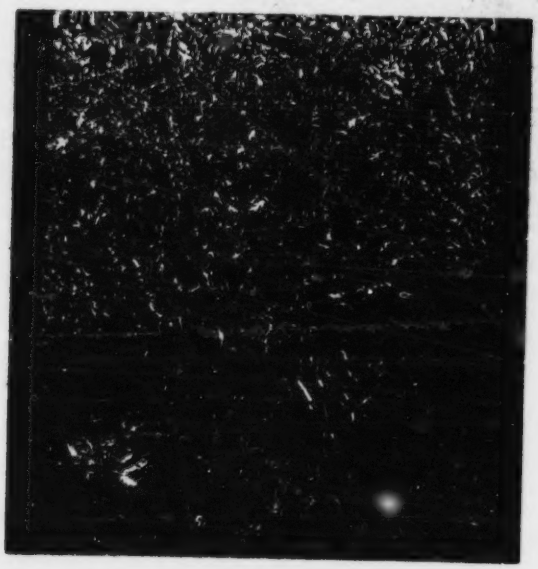

(b)

(c)

Fig. 23. Longitudinal section of the quenched interface of the Zn-27%Al alloy. $R = 5 \times 10^{-3}$ cm/sec, (a) solid-down, $G = 44^{\circ}C/cm$ (x13) (b) solid-up, $G = 56^{\circ}C/cm$ (x13), (c) solid-up, $G = 120^{\circ}C/cm$.

(a)

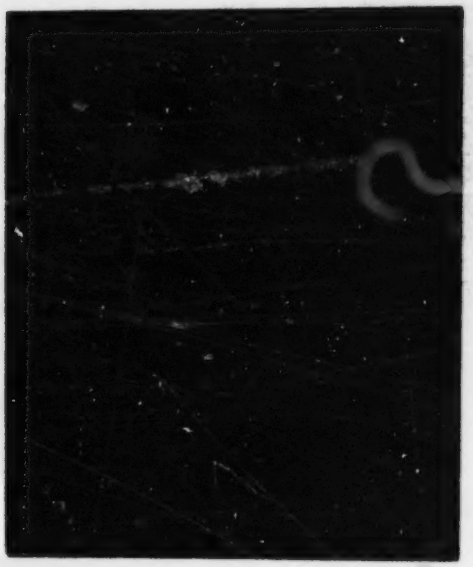

(b)

(c)

Fig. 24. Longitudinal sections of the quenched interfaces of the commercial alloys grown vertically upwards. $R = 5 \times 10^{-3}$ cm/sec, $G = 44°C/cm$ (x12) (a) ZA-8, (b) ZA-11, (c) ZA-27.

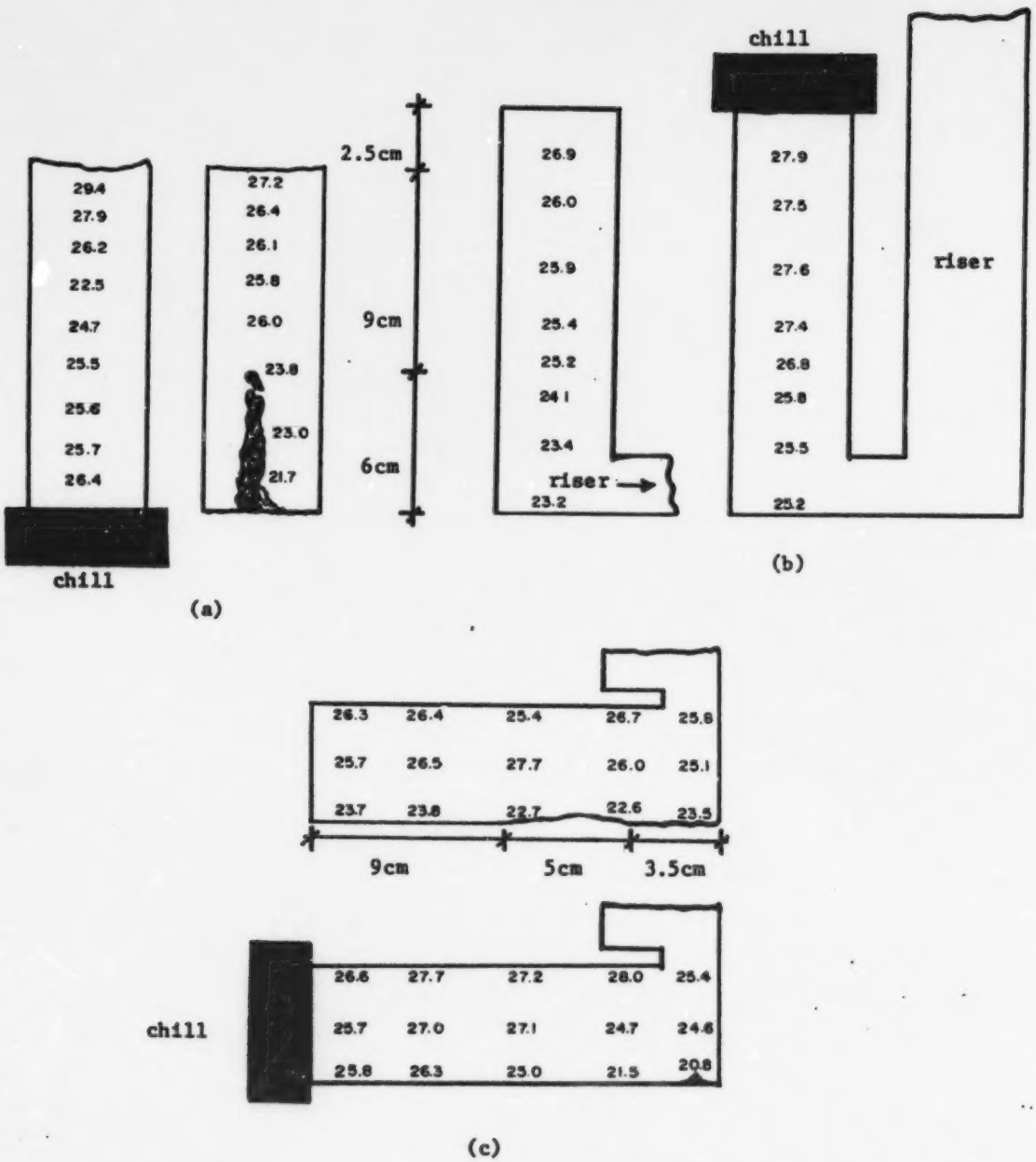

Fig. 25. Schematic drawings of the different casting configurations (ZA-27 alloy) with Al-concentration at various points.
(a) solid-down (b) solid-up (c) horizontal

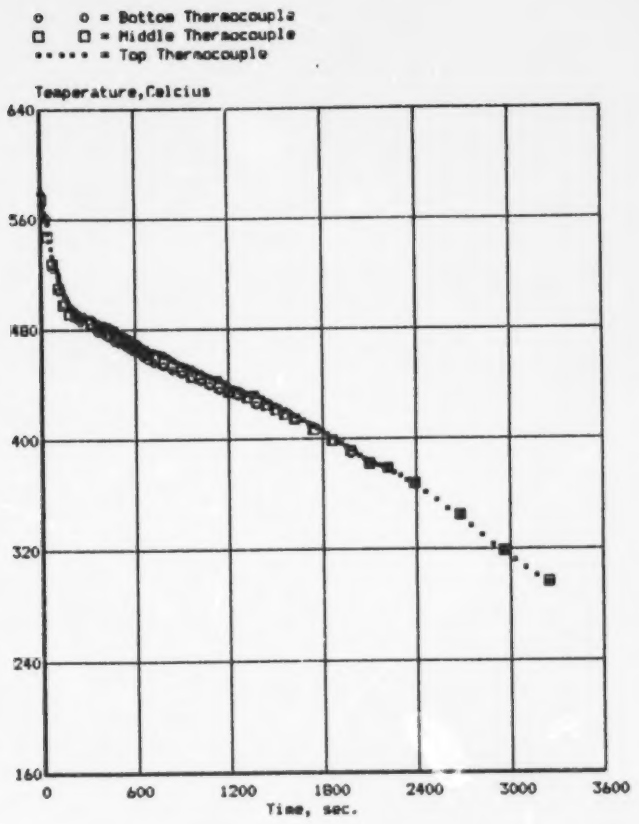

(a)

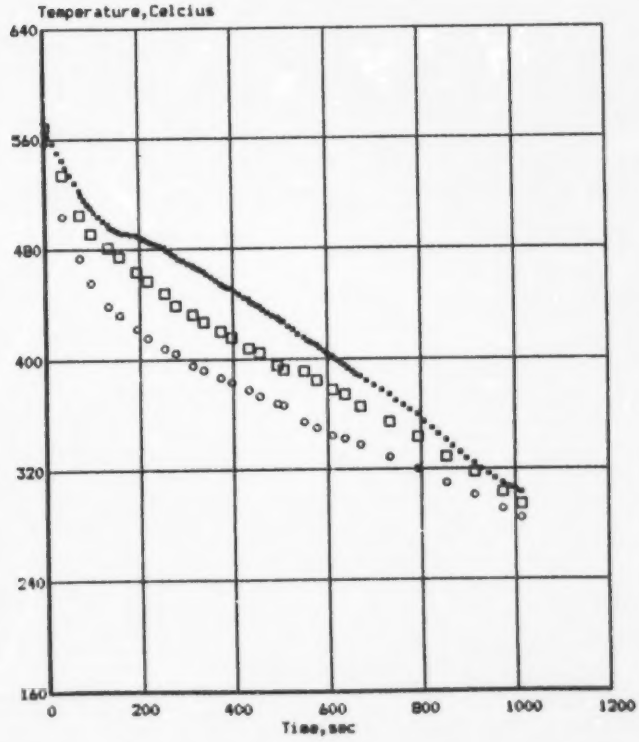

(b)

Fig. 26. Cooling curves (a) without chill (b) with chill. Commercial alloy, ZA-27.

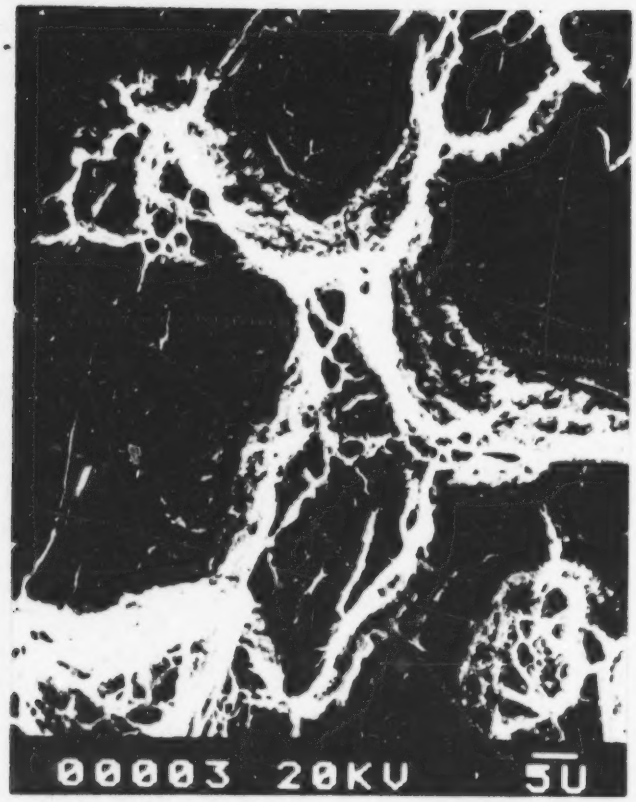

Fig. 27. SEM Micrograph of the fracture surface of the Zn-11%Al binary alloy.

(a)

(c)

(b)

(d)

Fig. 28. Microstructures of the ZA-12 (commercial) alloy
(a) Sand-cast (x100), (b) Chill-cast (x100),
(c) SEM (Sand-cast), (d) SEM (Chill-cast).

(a)

(c)

(b)

(d)

Fig. 29. Microstructures of the ZA-12 + 0.05% Ti alloy
(a) Sand-cast (x100), (b) Chill-cast (x100),
(c) SEM (Sand-cast), (d) SEM (Chill-cast).

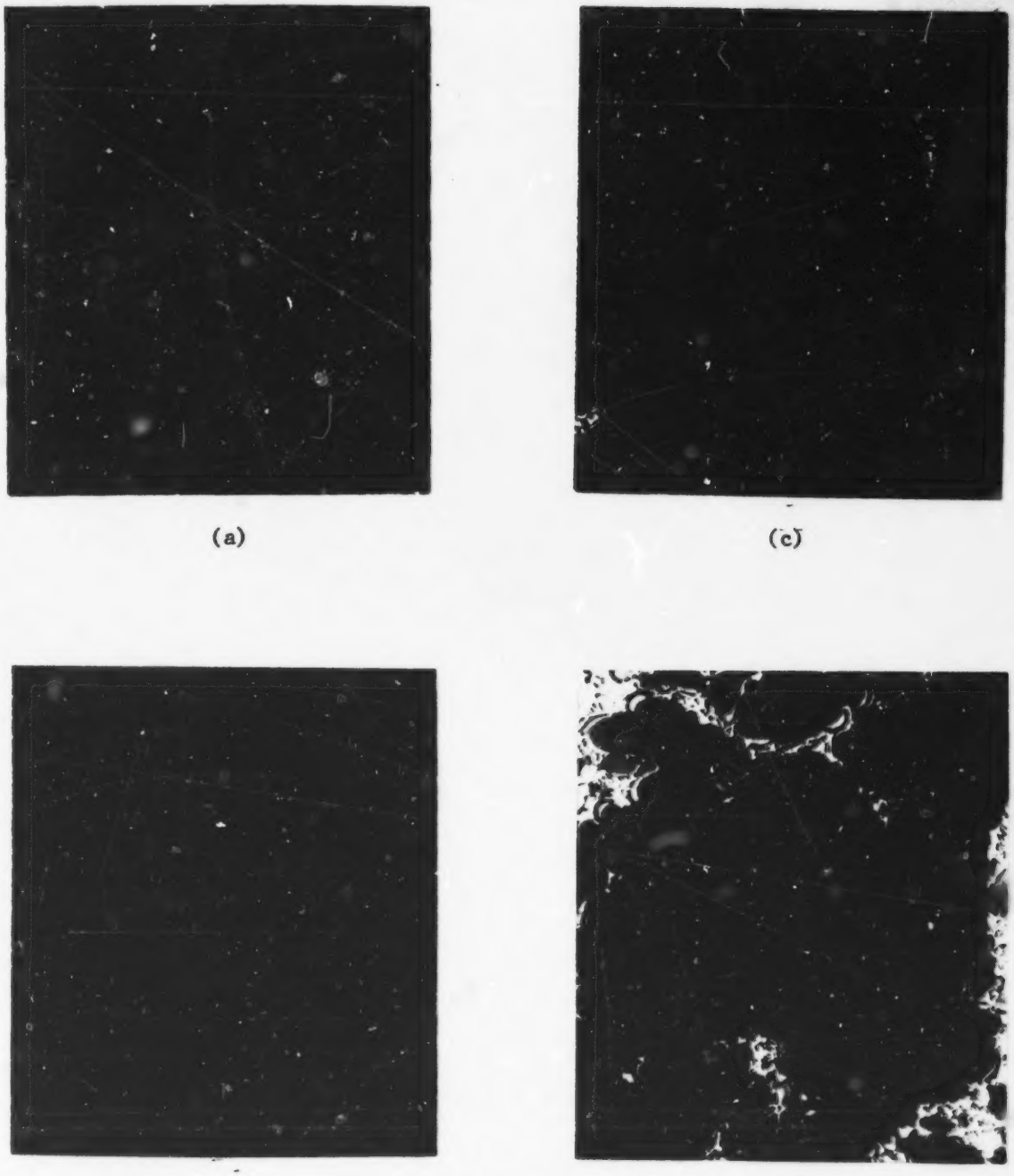

Fig. 30. Microstructures of the ZA-27 (commercial) alloy
(a) Sand-cast (x100), (b) Chill-cast (x100),
(c) SEM (Sand-cast), (d) SEM (Chill-cast).

(a)

(c)

(b)

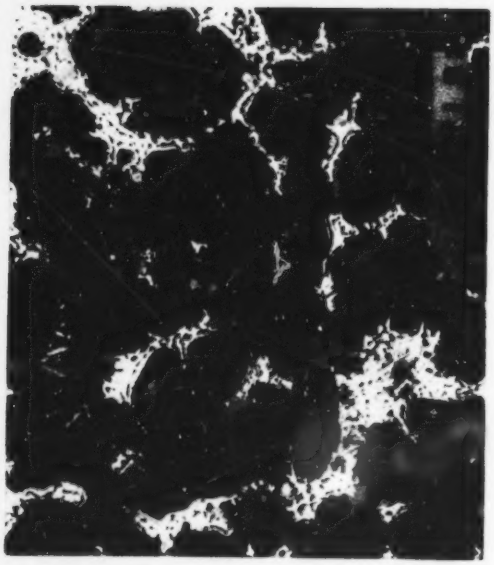

(d)

Fig. 31. Microstructures of the ZA-27 + 0.05% Ti alloy
(a) Sand-cast (x100), (b) Chill-cast (x100),
(c) SEM (Sand-cast), (d) SEM (Chill-cast).

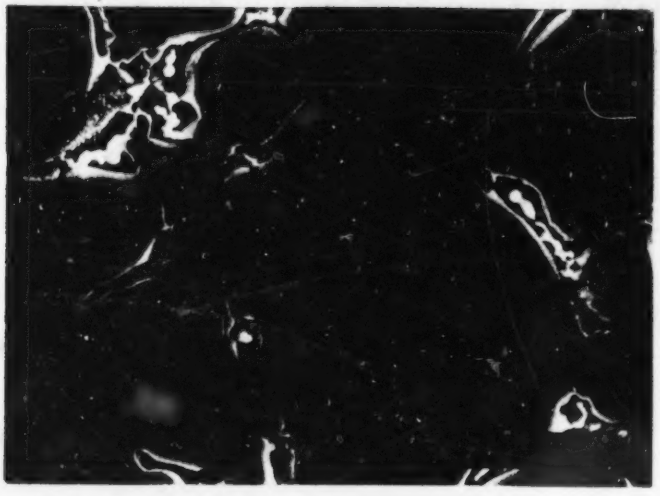

(a)

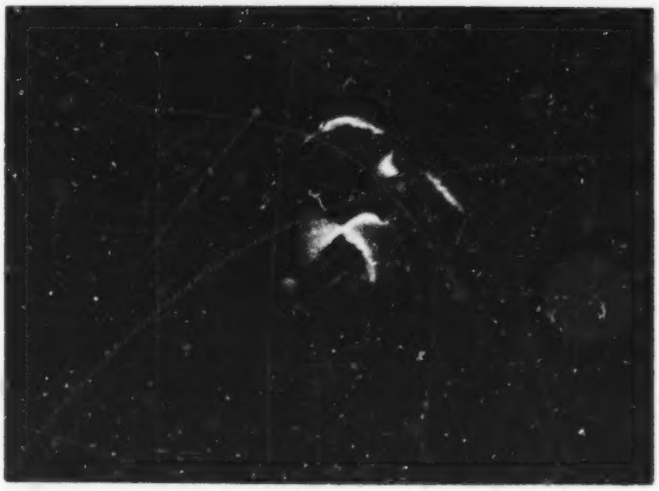

(b)

Fig. 32. Nucleating particle (Al_5Ti_2Zn) at the center of the primary Al-rich dendrite.
(a) low magnification
(b) high magnification.

(a)

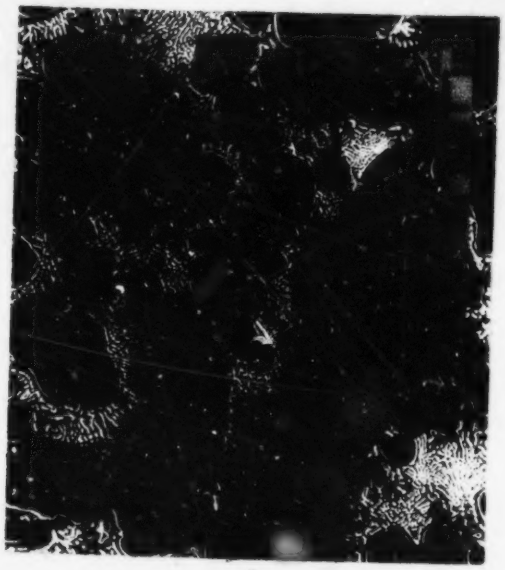

(c)

(b)

(d)

Fig. 33. Microstructures of the ZA-12 + 0.05% Zr alloy
(a) Sand-cast (x100), (b) Chill-cast (x100),
(c) SEM (Sand-cast), (d) SEM (Chill-cast).

(a)

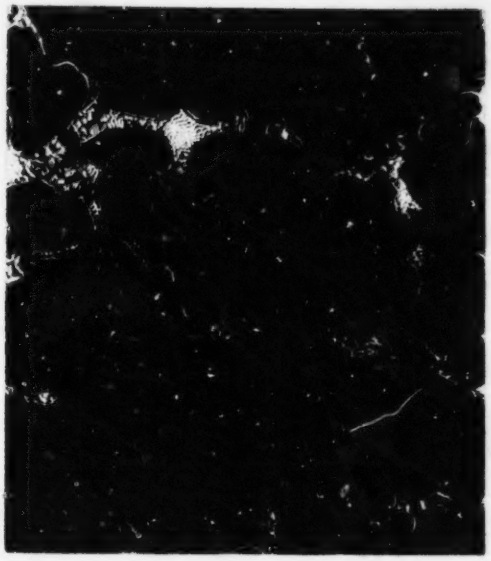

(c)

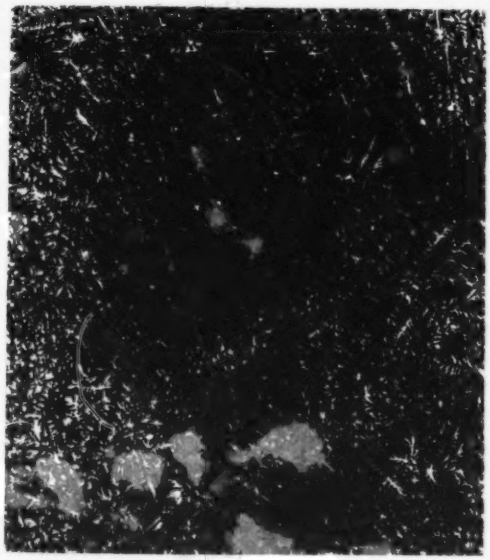

(b)

(d)

Fig. 34. Microstructures of the ZA-27 + 0.05% Zr alloy
(a) Sand-cast (x100), (b) Chill-cast (x100),
(c) SEM (Sand-cast), (d) SEM (Chill-cast).

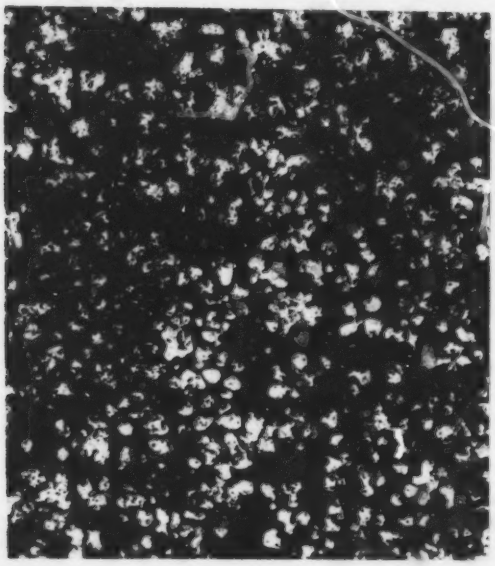

(a)

(c)

(b)

(d)

Fig. 35. Microstructures of the ZA-12 + 0.065% Ti + 0.013% B alloy
(a) Sand-cast (x100), (b) Chill-cast (x100),
(c) SEM (Sand-cast), (d) SEM (Chill-cast).

(a)

(c)

(b)

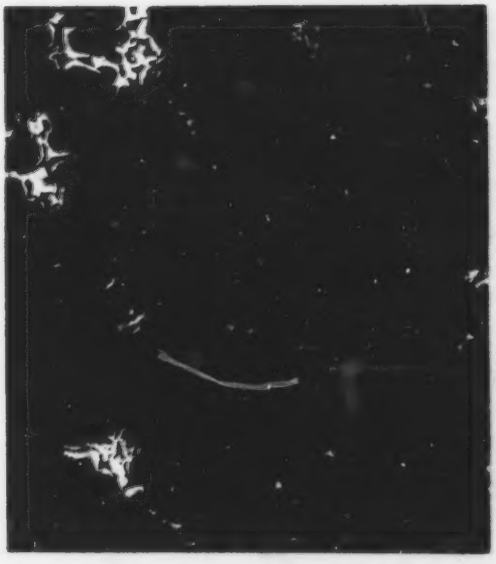

(d)

Fig. 36. Microstructures of the ZA-27 + 0.065% Ti + 0.013% B alloy
(a) Sand-cast (x100), (b) Chill-cast (x100),
(c) SEM (Sand-cast), (d) SEM (Chill-cast).

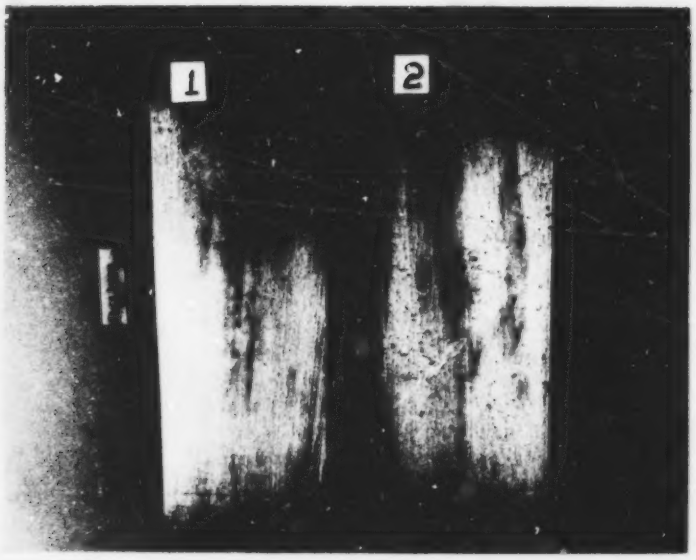

Fig. 37. Green sand mold: 1- Non-stirred 2- Stirred immediately after pouring.

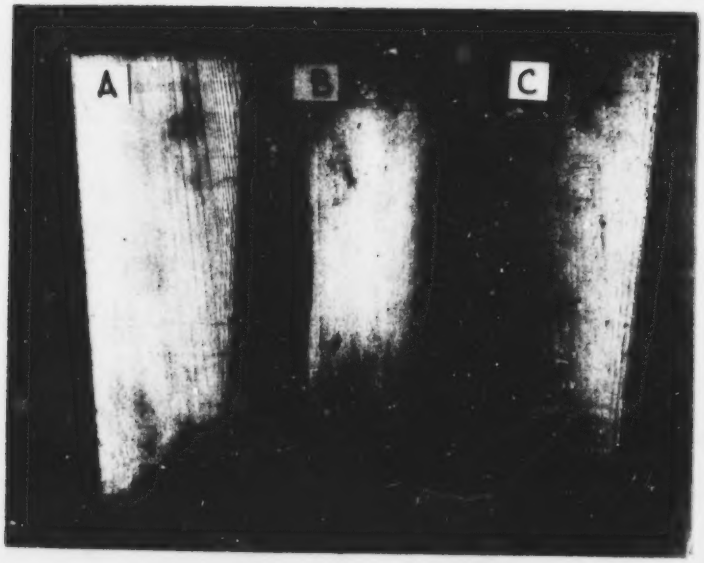

Fig. 38. Ceramic mold (heatd up to 600°C)
A non-stirred B stirred with the magnetic force downward
C stirred with the magnetic force upward

(a)

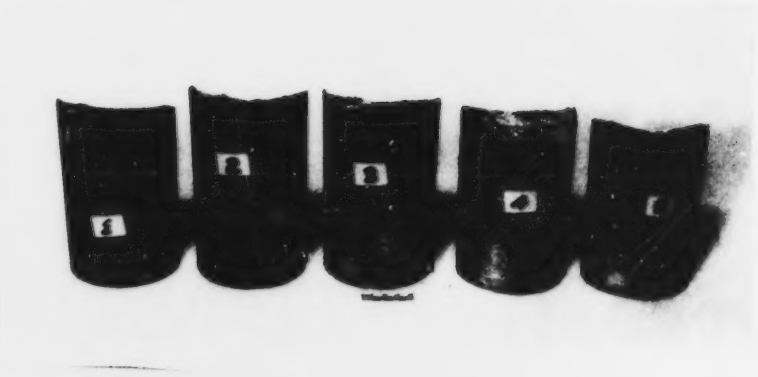

(b)

Fig. 39. Large size ingots: a - Longitudinal section b - Side view.

1. Non-stirring
2. The stirrer was switched on immediately after pouring
3. The stirrer was switched on 30°C below the liquidus (455°C)
4. The stirrer was switched on 10°C above the liquidus (495°C)
5. The stirrer was switched on 10°C below the liquidus (475°C)

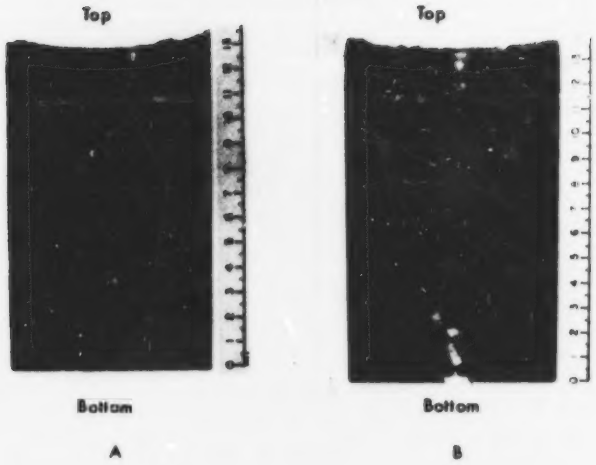

Fig. 40. Longitudinal section of ingots of the Zn-27%Al showing the locations of samples taken by drilling for chemical analyses (a) unstirred ingot (A1) (b) stirred ingot (Q4).

(a)

(b)

Fig. 41. Micrographs from the various positions in the unstirred ingot (see Fig. 33A)
(a) The spot number 7 (i.e. the top of the ingot)
(b) The spot number 1 (i.e. the bottom of the ingot). (x100).

(a)

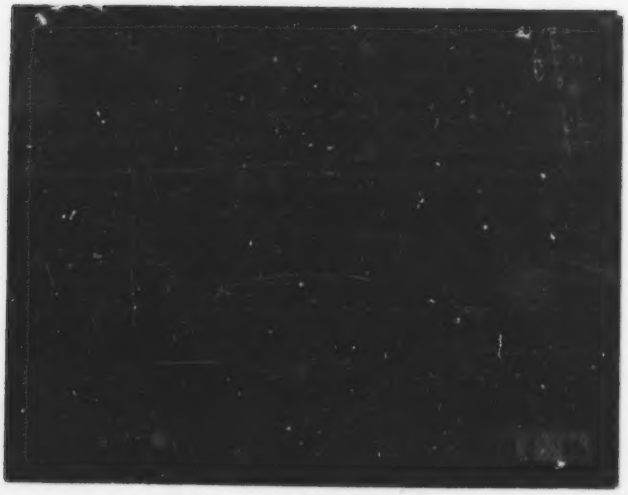

(b)

Fig. 42. Micrographs from the various positons in the unstirred ingot (see Fig. 33B).
(a) The spot number 8 (i.e. the top of the ingot)
(b) The spot number 1 (i.e. the bottom of the ingot). (x100).

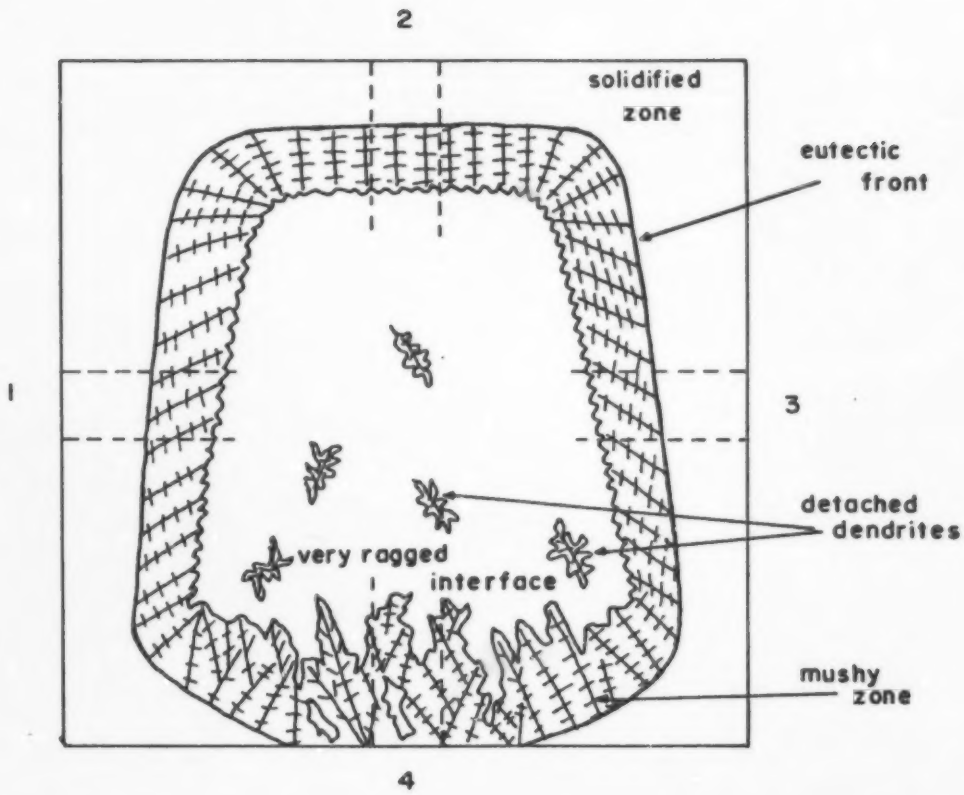

Fig. 43. Schematic illustration of the solid liquid interface in a casting.

Table 1: Comparative Properties of Foundry Alloys

	ZA-12		ZA-27		ZA-8		Bronze (85-5-5-5)	Aluminum (356-T6)	Cast Iron (Class 30)
	Sand	Perm Mold	Sand	Sand HT	Sand	Perm Mold	Sand	Sand	Sand
Ultimate tensile strenth (MPa)	275-310	310-345	400-441	310-325	255-268	270-248	255	227.5	206-234
Yield Strength (MPa)	206	214	365	255	193	206	117	165.5	---
Tensile Elongation %	1-3	1-3	3-6	8-11	1-2	1	30	35	---
BHN	105-125	105-125	110-120	90-100	90-10	85-90	50-60	70	179
Young Modulus (MPa)	82.75	82.75	75.00	75.00	85.5	85.5	93	72.5	89.5
Density (g/cm^3)	6.03		5.00		6.3		8.80	2.68	7.196
Solidification Temp. Range (°C)	432-377		487-375		404-375		854.5-1009.5	580-610	1149-1204.5
Electrical Conductivity % IACS	28.3		29.7		27.7		15	40	

Table 2: Composition of the Commercial Alloys (wt%)*

Alloy	Al	Cu	Mg	Fe	Si	Zn
2803 (ZA-12)	12.0	1.06	0.015	0.032	0.01	Balance
2805 (ZA-8)	7.59	1.17	0.02	0.032	0.01	Balance
2806 (ZA-27)	26.14	2.21	0.016	0.16	0.3	Balance

* Analyses were performed in CANMET Laboratories.

Table 3: Composition (wt%) of the Commercial Alloys

Alloy #	Al	Cu	Mg	Fe	Si	Zn
2630-2 -3	8.26	1.20	0.018	0.037	----	Balance
2629-2 -3	10.9	1.13	0.018	0.034	0.01	Balance
2621-1	27.6	2.06	0.018	0.087	0.01	Balance
2625-1	26.7	2.32	0.013	0.12	0.01	Balance

Table 4: Composition in Various Positions of the Unidirectionally Solidified

	Composition (wt% Al)		
Sample	Bottom	Middle	Top
$R = 10^{-1}$ cm/sec, solid-down	25.75	----	30.25
$R = 10^{-2}$ cm/sec, solid-down	19.60	----	29.70
$R = 10^{-1}$ cm/sec, solid-up	24.30	26.80	29.20
$R = 10^{-2}$ cm/sec, solid-up	24.10	----	30.40

Table 5: Mechanical Properties of the Directionally-grown Binary Alloys

Alloy*	0.2% Offset Yield Strength (MPa) Tensile	Compressive	U.T.S. (MPa)
Zn-8%Al, solid-up	50.5	140.13	158.2
Zn-11%Al, solid-down	74.5	155.30	158.3
Zn-11%Al, solid-up	51.0	177.47	169.7
Zn-27%Al, solid-down	64.07	240.15	240.
Zn-27%Al, solid-up	81.4	257.44	253.6
Zn-8%Al, solid-down	----	145.33	----

* R (Growth rate) = 10^{-2} cm/sec

Table 6: Mechanical Properties of the Directionally-grown Commercial Alloys

Alloy	0.2% Offset Yield Strength Reported tensile* (MPa)	Compressive (MPa)	U.T.S. (Reported MPa)
2805 (ZA-8) solid-down	(206)**	319.68	(220-255)*
2805 (ZA-8) solid-up		281.17	
2803 (ZA-12) solid-down	(255)	372.71	(310-325)
2803 (ZA-12) solid-up		383.20	
2806 (ZA-27) solid-down	(365)	498.62	(400-440)
2806 (ZA-27) solid-up		495.70	

Growth rate = 5 x 10^{-3} cm/sec, grown in air.
* Sand Cast
** Permanent Mold

Table 7: Mechanical Properties of the Commercial Alloys

Alloy	Compressive Strength (0.2 offset)	Tensile Strength (0.2 offset) Reported	U.T.S. Reported
2630-2	274.01	(200)	(252)
2630-3	291.83		
2629-2	295.98	(230)	(299)
2629-3	279.60		
2625-1	412.97	(365)	(400-440)
2621-1	407.67		

Table 8: Composition* in Various Positions of the Stirred and Unstirred Ingots (Zn-27%Al)

Sample Description	wt % Al	
	Unstirred (Q1)	Stirred (Q4)
1	22.1	26.6
2	26.4	26.4
3	28.8	26.0
4	28.7	27.6
5	29.7	28.6
6	29.9	28.7
7	30.0	30.1
8	----	30.5

*Chemical analyses were performed in CANMET Laboratories in Ottawa.